REACTOR COOLANT SYSTEM
ASYMMETRIC LOCA LOAD EVALUATION

REVISION 1

ST. LUCIE UNIT 1 - DOCKET NO. 50-335

July 31, 1980

TABLE OF CONTENTS

TABLE OF CONTENTS (Cont'd)

TABLE OF CONTENTS (Cont'd)

SUMMARY

In May 1975, the NRC Staff was informed by a pressurized water reactor licensee that loads resulting from a hypothetical rupture of the reactor coolant cold leg pipe in the immediate vicinity of the reactor pressure vessel (RPV) may have been underestimated.

In November 1975, the Staff agreed that these loads should be considered and evaluated on a generic basis.

Florida Power & Light's response to the Staff's letter of November 26, 1975 indicated that the support system design incorporated the reaction forces associated with the large arbitrary reactor coolant pipe ruptures, and that further, it had been shown to acceptably accommodate the additional loads associated with differential pressures within the reactor cavity as shown in Appendix 3H of the Final Safety Analysis Report.

The Staff requested that further internal asymmetric load (IAL) evaluations be conducted. FP&Ls letter of February 9, 1976 documents the Company's commitments to evaluate the reactor vessel support capability for the limiting break, a commitment which is restated in Supplement 2 to the Unit 1 Safety Evaluation Report (SER), dated March 1, 1976.

In September 1977 FP&L transmitted to the NRC a report assessing the margin in design of the vessel supports when the internal asymmetric loads are added to all previous loads. The report concluded that the supports would adequately withstand all the loadings. However, since the analysis did not account for gaps between the vessel and the core barrel, and also the vessel and the support structures, an analysis was initiated at the same time to account for these effects.

The Staff's letter of February 16, 1978 requested that the evaluations conducted to date be expanded in scope to include an assessment of the reactor pressure vessel, fuel assemblies and internals, control element assemblies, primary coolant piping and attached ECCS piping, all primary system supports, and the biological and secondary shield walls for a spectrum of breaks in the primary system. FP&Ls March 1978 response stated that its August 1977 report was fully responsive to the Staff's SER requirement, that the St. Lucie 1 design was acceptable and that the large instantaneous pipe breaks being postulated were overly conservative. The response went on to say that FP&L would pursue additional analyses once the Staff approved the analytical methods used in the August 1977 report. This reply notwithstanding, FP&L being sympathetic with the Staff's desire to assess any potential risk to public health and safety from postulated events, expanded the analysis referred to above, to also assess the additional items identified by the Staff.

This report discusses the results of this expanded analysis. The combination of thrust, external, and internal asymmetric loads resulting from the inlet

pipe circumferential break present the largest load to the vessel supports among those that would ensue from any of the design basis breaks listed in Appendix 3H of the FSAR.

The results confirm that the vessel supports will adequately withstand all the loads resulting from the postulated physically possible circumferential break in the vessel inlet pipe. The cold leg guillotine break in the cavity is the break which results in the largest loading of the vessel supports. Therefore the vessel supports are clearly adequate for all other break locations. This reaffirms the conclusions of the August 1977 report.

Results also show that all supports for the primary system are adequate for all break locations, that the stresses in the intact primary piping and attached lines are sufficiently low to ensure performance of intended functions, and that the biological shield wall performs its intended function. The secondary shield wall is designed for postulated primary system ruptures within the steam generator subcompartments.

Results further show that the control element assemblies, which are not needed for the postulated breaks, maintain the pressure boundary integrity when subjected to the motions resulting from those breaks. Analyses of the adequacy of the reactor internals and fuel were performed using a slightly different hydraulic model to compute the forcing functions to be applied to the said internals and fuel. The forcing functions took no consideration of limitations in break area other than may be due to the strength of the primary piping itself. This was done to take advantage of these very same analyses performed for a virtually identical plant, Calvert Cliffs, recognizing that results thus obtained would be bounding those that would be computed for the breaks physically possible in St. Lucie 1. The results of the reactor internals analyses demonstrate that the internals are capable of accommodating loads resulting from the largest cold and hot leg breaks. The analyses of the fuel indicates that for an unrestrained inlet break localized crushing of the grid spacers occurs near the top of some of the peripheral assemblies. However, this limited crushing does not prevent maintaining the coolable geometry of the assembly and the core overall.

It must also be noted that since the submittal of the August 1977 report to the Staff, additional work has been reported to support FP&Ls contention that the types of instantaneous pipe breaks being postulated by the Staff are excessively conservative.

1.0 INTRODUCTION

During a postulated loss of coolant accident thermodynamic and hydrodynamic induced loads occur throughout the primary system. When the loss of coolant accident is in the form of a circumferential pipe rupture at the inlet nozzle of the reactor pressure vessel, a decompression of the reactor pressure vessel occurs over a short period of time. Decompression waves which originate at the postulated break travel around the inlet plenum and propagate downward along the downcomer annulus. The finite time required by the decompression disturbances to travel about the vessel causes a transient pressure differential field to be created across the core support barrel (CSB) and the vessel inner surface. This field imposes a transient asymmetric loading on the core-support-barrel as well as the vessel itself. Since the postulated pipe break is located within the biological shield wall, the blowdown fluid flashing into the reactor cavity also causes a transient pressurization acting on the vessel. This external pressurization is also asymmetric (EAL). The internal asymmetric loading (IAL) and the external asymmetric loading act in the same direction for breaks occurring in the cold leg piping. For breaks in the hot legs, the internal asymmetric load is virtually absent in the horizontal direction, hence the two loads are additive in the vertical direction only. These loadings are transmitted to the reactor vessel support system. The resultant reaction forces at the support interfaces must be considered in the evaluation of the adequacy of the support system together with the thrust load resulting from the break and other operating loads. Normal operating loads, together with postulated seismic loads, as well as the EAL have been previously analyzed in Appendix 3H of the Final Safety Analysis Report.

Breaks outside the reactor cavity can result in IAL imposed on the reactor pressure vessel and internals, and in EAL on the reactor coolant pump and steam generators.

For the breaks outside the cavity, the adequacy of the primary system supports is assessed for full breaks at appropriate primary system locations. The cavity breaks are the determining breaks for the assessment of the adequacy of piping attached to the primary system piping.

The circumferential pipe rupture at the inlet nozzle of the reactor pressure vessel is determined to be the design basis break for the evaluation of the vessel support adequacy. A break at the outlet nozzle would not produce a horizontal asymmetric pressure loading to the vessel. Consistent with the Final Safety Analysis Report, a 4.0 square foot cold leg guillotine break at the inlet nozzle is chosen for the analyses of the vessel support adequacy and for the other analyses conducted by Ebasco; namely, the assessment of the adequacy of the coolant piping, the control element drives, the ECCS piping and the biological shield wall. Because of virtual identity of the vessel internals and fuel with other plants for which an analysis had been performed, a bounding analysis utilizing a full size (1414 in^2) cold leg break at the inlet nozzle has been performed by Combustion Engineering to assess the adequacy of the reactor internals and the fuel. The hot leg guillotine ruptures develop less than full area breaks because of the inherent strength of the hot leg piping and the stiffness of the supports of the major components.

The break area resulting from a hot leg guillotine at the vessel nozzle is approximately 135 in^2.

2.0 METHOD OF ANALYSIS

The methods of analyses employed to ascertain the adequacy of the vessel supports, vessel internals, fuel, primary piping, attached piping, control rod drives, and biological shield wall are discussed in the subsequent sections. The required analyses have been performed by Ebasco Services, Inc. and Combustion Engineering, the latter being responsible for the analyses of the reactor vessel internals and the fuel. Although the analytical methods employed are similar, there are some differences in assumptions. These differences however do not invalidate the results and they are discussed in detail where necessary.

2.1 Reactor Vessel Supports

The adequacy of the reactor vessel supports is evaluated by determining the loads acting on the primary system which result from a postulated break at the inlet cold leg nozzle; the response of the primary system to the application of these loads; and the reaction forces generated by this response at the reactor vessel supports. The loads acting on the primary system consist of normal loads, the thrust load, external asymmetric loads, and internal asymmetric loads. The latter three are combined in true time history fashion and added to the normal loads reactions. The resultant reaction loads at the supports have been combined with design reaction loads resulting from the postulated seismic (SSE) events by SRSS techniques, to obtain the overall reaction load at each of the supports. This has been done for the analysis of the vessel supports as a continuation of the analyses presented in Appendix 3H of the FSAR, which included seismic loads, so that the combined loads are applied as peak static loads to the biological shield wall. The Staff, at a meeting in January 1980 further requested that seismic loads be separately identified. Design seismic loads are provided for each primary system support in the three orthogonal directions in Table 1. It should be emphasized that computed peak siesmic loads are, in general, substantially less than the design seismic loads; thus providing an element of conservatism in this analysis. Table 2 gives a sample comparison of calculated and design seismic loads at representative locations.

The following subsections describe the methodology employed to evaluate each of the thrust, external asymmetric and internal asymmetric loads. Inherent in the evaluation of these loads is the determination of the time required to open up the break to the area being analyzed.

2.1.1 Break Opening Time and Thrust Loads

The St. Lucie Plant primary coolant piping in the vicinity of the vessel is restrained from unlimited motion following complete severance in the portion

within the cavity by restraints in the primary shield wall penetrations and wire ropes around the reactor coolant pumps. This restraining system has been previously described in the FSAR. Following an arbitrarily assumed instantaneous severance of the pipe at the nozzle, the two ends of the broken pipe separate under the action of the thrust imposed by the instantaneous tension release followed by the blowdown of the escaping fluid, and form a combined break area which varies with time as given in the following equation:

$$A_b(\tau) = \frac{\pi R_i \beta x(\tau)}{45} + 2R_i^2 \left[\pi - (\frac{\beta\pi}{90} - \sin 2\beta\right] - \frac{\pi\beta(R_i+R_o)t}{180} \quad (1)$$

where R_i and R_o are the inner and outer pipe radii, t is the pipe thickness, x is the axial separation of the two ends which varies with time τ, and

$$\beta = \cos^{-1} \frac{y(\tau)}{2R_i} \quad (2)$$

wherein y is the radial separation of the two broken ends which also varies with time.

This equation is solved in iterative fashion together with the equation for the combined tension release and blowdown force, given below

$$F(\tau) = P_{dl}(\tau)A_p + \rho_{dl}(\tau)A_b(\tau)\frac{V_e^2(\tau)}{g} \quad (3)$$

to yield the correct forcing function and break area as a function of time. In equation (3), P_{dl} and ρ_{dl} are the pressure and fluid density in the discharge leg, respectively, A_p is the cross-sectional area of the pipe, V_e the blowdown velocity, and $A_b(\tau)$ is defined in (1) above.

The motion of the pump discharge portion of the primary piping system under the application of the force given by (3), is computed by modelling the discharge leg, the pump, and the cross over leg with an elasto-plastic finite element computer program, PLAST [1] considering the steam generator and the vessel to remain motionless.

Results of the analyses indicate that at least 18 msec. are necessary for the pipe ends to separate to the overall area of 4.0 square feet referred to in the FSAR. This analysis also indicates that as a result of plastic rotation at the pump, it is possible for the pipe ends to separate further, to a maximum area of 7.78 square feet. The time required for this area to be achieved, however, would be in excess of 25 msec. The longer time required

for opening the larger break insures that the IAL resulting from the two breaks are virtually identical. The larger break does however result in a larger external horizontal asymmetric load (external vertical asymmetric loads are virtually identical for the two breaks). Since the 4.0 square foot break had been one of the design basis breaks in the FSAR, all analyses, except for fuel and internals, used that break area, consideration being given however to whether the system is capable of accommodating the larger break. For the fuel and reactor internals, the full 1414 in^2 guillotine break at the discharge leg vessel nozzle was used in the analysis and the results were used to bound those for the smaller physically possible breaks. The 1414 in^2 cold leg guillotine break used in the analysis of the internals and fuel has been conservatively assumed to open to its full size in 23 msec. In reality, the time will be longer. The break opening time for the 135 in^2 hot leg break has been calculated to be in excess of 20 msec.

These times have been computed utilizing a three-dimensional model of the reactor coolant system using lumped mass parameter techniques. The mathematical model represents the total reactor coolant system mass and stiffness, with discontinuities at the reactor vessel inlet and outlet breaks, respectively. The two models are shown in Figures 19a and 19b. No restraints in the cold leg piping are included in this model, which is somewhat different than that employed to solve for the opening time of the restrained inlet piping break. The physical definition of the models shown in Figures 19a and 19b have been supplied in the STRUDL Code[5], which generated the condensed stiffness matrix. This matrix, along with the mass definition, gapped support definition, damping and the time history forcing functions previously discussed, has been supplied to the DAGS Code [7], which in turn has generated the severed pipe end and the safe end displacement history. As discussed in the subsequent section, the system is adequate for the largest of the physically possible breaks.

2.1.2 External Asymmetric Pressure Loads (Reactor Cavity)

The reactor subcompartment analysis for St. Lucie Unit 1 has been performed for stipulated LOCA conditions including a 4.0 square foot cold leg guillotine break, and the results had been submitted to the NRC in the FSAR and approved by the NRC during the course of the operating license review. The results for the 4.0 square foot cold leg guillotine break, as reported in Reference 2, have been directly used in the present study for the assessment of the adequacy of the vessel supports, the ECCS lines, the CEDM's and the biological shield wall. The internal asymmetric loads on the fuel and reactor internals were conservatively determined by using the results obtained for a full size break in the inlet line of a generic plant (Calvert Cliffs) representing the St. Lucie 1 plant; for consistency, the assessment of the fuel and internals adequacy also employed a cavity pressure resulting from a full 1414 in^2 inlet break. The Reference 2 analysis overestimates the EAL for the 4.0 square foot break since the cavity response had been predicated on a break opening time of 10 msec.; whereas, 18 msec. is needed to achieve this size break. The peak external asymmetric forces across the reactor vessel, that would result from the largest physically possible 7.78 square foot break, would be approximately 40 percent larger. This is predicated on a ratio of 1.39 between peak and average energy flow to the cavity resulting from a 7.78 square foot and a 4.0 square foot cold leg break, respectively.

In the original analysis, however, two elements of conservatism had been introduced. First, the mass and energy releases had been increased by 10 percent and second, all insulation had been assumed to remain in place in the reactor cavity for the purposes of volume and vent area calculations in the mathematical model. The insulation in the upper cavity reaches would have to be crushed against the vessel upon cavity pressurization prior to transmitting the loads to the vessel, resulting in an increased volume of approximately 15 to 20 percent.

Hence, realistic modelling of the insulation behavior, coupled with removal of the 10 percent conservatism in the mass and energy release would result in a predicted external asymmetric pressure load and cavity pressure load from a 7.78 square foot break which is only 15 to 20 percent higher than those conservatively predicted.

2.1.3 Internal Asymmetric Pressure Loads

The model used to determine the pressure field at every point in the primary system following the postulated primary system breaks, from which the internal asymmetric forces on the vessel and core support barrel are deduced, is shown in Figure 1. This model is used for the vessel support, CEDMs, ECCS lines and biological shield wall assessment.

The RELAP-4 [3] thermal hydraulic code is used to compute the thermodynamic properties in the model volumes and junctions. Results of the RELAP-4 model have been compared to results achieved by modelling the system with WHAM-6 [4] for the period of time during which the latter can be applied with confidence, which is also the period of time of interest. Figure 2 shows the model employed for WHAM-6. A similar WHAM model and assumptions in its use, had been previously submitted to the Staff in the August 1977 report. The results of the two models are in good agreement, with RELAP-4 predicting a larger pressure differential across the core support barrel.

Results of the internal asymmetric loads analysis indicate that the peak forces across the core support barrel and the vessel are virtually insensitive to the break area, but extremely sensitive to break opening times. For instance, a change in area from 1 square foot requiring 8 msec. to open to approximately 9.81 square feet (complete double-ended area break) with an opening time of 36 msec., only results in a 2 to 3 percent increase in peak internal asymmetric loads, whereas, a decrease in opening time from 36 msec. to 1 msec. for the full break brings about a threefold increase in internal asymmetric load.

The pressure fields, flow rates and density distributions in the case of the hot leg breaks and the full size (1414 in^2) cold leg break, used for the assessment of the internals and fuel have been computed with the CEFLASH-4B computer code according to the methods documented in Reference 19.

2.1.4 Vessel and Primary System Structural Model

A non-linear elastic time history dynamic analysis of three-dimensional mathematical model of the reactor coolant system including details of the reactor

internals, pressure vessel, supports, and piping was performed for the postulated pipe break to provide reactor vessel support reaction forces.

The structural model employed is shown in Figures 3(a) and 3(b). This model is three-dimensional and has 981 total static degrees of freedom and 77 mass degrees of freedom. The reactor vessel and all internal components are modelled at internal and support interfaces.

The STRUDL [5] computer code generates the condensed stiffness matrix used in the dynamic analysis from the physical definition of the structure. Hydrodynamic effects, including both virtual mass and annular effects are accounted for in the coupling between the reactor pressure vessel (RPV) and the core support barrel (CSB) and between the CSB and the core shroud. The hydrodynamic (added) mass matrix is evaluated using the ADMASS [6] code.

The dynamic analysis to determine the system response was performed using the computer codes DAGS [7] and DFORCE [8].

The reactor pressure vessel support system is described in the FSAR. The modelling of the steel portion of the support is identical to that described in the FSAR in Appendix 3H. The basic model of the biological shield wall is also identical. However, a more refined analysis is employed for the latter, utilizing a NASTRAN [9] nonlinear solution procedure employing quadrilateral and triangular plane stress concrete cracking finite elements, instead of the STARDYNE method of solution described in Appendix 3H of the FSAR.

The structural model employed for the determination of the loads to be used in the evaluation of the reactor vessel internals and the fuel differs in some minor details from that presented in Figures 3(a) and 3(b), but is substantially the same, as shown in Figure 15. The latter model had already been developed for a plant (Calvert Cliffs) which is nearly identical to St. Lucie 1, and that model was therefore utilized.

2.2 Reactor Coolant Piping, Connected Piping and Other RCS Supports

2.2.1 Steam Generator Supports

Outside the reactor cavity, breaks have been assumed at appropriate locations.

The RCS supports most affected are the lower steam generator supports.

The primary system model is analyzed on an elastic basis for both hot leg and cold leg breaks, the hot leg break at the steam generator inlet being the determining event for the Steam Generator support.

This analysis is a static analysis which employs the computer code MEC-21 (Mare Island Piping Flexibility Code) [12].

Both LOCA and design seismic loads are included in the analysis since the design seismic loads had been included during initial design.

2.2.2 ECCS and Other Connected Piping

The analysis of the stresses generated in the ECCS lines and other lines attached to the primary loop involved a two step process. First, the time histories of the displacements are generated at each nozzle attaching said piping to the primary loop. The "worst" time history, irrespective of the location at which it occurs is applied to the line which by configuration and other loading (normal and seismic) would result in the highest stresses. The stresses induced by LOCA motions for this particular configuration are added to previously computed normal and seismic (SRSS) stresses since design loads had the seismic loads already combined. The determining break for ECCS line evaluation is the cold leg nozzle break in the cavity.

2.2.3 Reactor Coolant Piping

The structural model for the primary system is also utilized to determine the stress conditions in the intact portion of the reactor coolant loop.

2.3 Reactor Internals

The postulated pipe breaks in the reactor cavity result in horizontal and vertical forcing functions on the internals and core. These loads are generated by the pressure gradients discussed in the previous sections and also by drag loads on the components. This section describes the hydraulic models used to compute drag induced forcing functions and the structural models used for determining the response of the internals and the fuel to the transient pressure and drag loads. These loads cause certain components to respond to both beam and shell modes.

2.3.1 Drag Loads

During a rapid blowdown strong rarefaction pressure waves travel through the reactor primary system resulting in large pressure gradients across various reactor internal components. These pressure gradients, in turn, result in an acceleration (deceleration) of the primary circuit fluid which causes an increase (decrease) in the associated component drag load. The loads resulting from the depressurization are discussed in Section 2.1.3. The subsequent sections explain how the drag loads have been evaluated.

2.3.1.1 CEA Shroud and Upper Guide Structure Drag Loads

During a blowdown the flow from the upper guide structure and into the hot leg nozzles undergoes a rapid change in magnitude and, possibly, direction. These give rise to trnasient drag loads on the individual control element assembly (CEA) shrouds and to a total load on the upper guide structure (UGS). These loads add to the transient pressure loads (which for the case of the CEA shrouds consist of an inertial component). The analysis of drag loads

has been performed for a generic plant (Calvert Cliffs) which is quite similar to St. Lucie 1 and for which the cross-flow drag factors were determined. The drag factors on the UGS were determined from a flow model experiment. The experimental data was scaled to represent the actual forces on a reactor UGS. The scaling factors consisted of geometrical scale factors as well as the transient momentum parameters for the hot leg nozzles as computed with the CEFLASH-4B Code [19].

The drag factors for the generic plant representing St. Lucie have been developed from geometrically similar experimental data as normalized drag force per unit axial length of CEA shroud at several discrete axial elevations. Forces have been normalized with respect to νW^2 (momentum parameter) of the scaled reactor outlet nozzle. The drag factors have been developed in order to give cross-flow loads on individual CEA shrouds and, by appropriate summation, on the entire upper guide structure.

2.3.1.2 Core Drag Loads

Separate loads are calculated for individual nodes representing the fuel rods, guide tubes, upper end fitting, and lower end fitting. Loads are obtained based on a control volume approach utilizing an integrated fluid momentum equation. Drag loads are represented by the fluid shear term in this equation.

Drag loads are composed of two components -- frictional drag and form drag. Frictional drag is calculated using a friction factor which is dependent on the channel equivalent diameter, channel cross-sectional area, fluid flow rate, and fluid density. The latter two quantities are obtained from CEFLASH-4B output. Friction factors are obtained using Colebrook's correlation which is an analytical representation of the Moody chart; this formulation requires the surface roughness and time dependent Reynolds' number. Form drag is calculated using a loss factor, along with channel area and equivalent diameter, and fluid density and flow rate. An experimentally determined correlation of loss factor as a function of Reynolds number is used. Crud effects are accounted for by multiplying the drag loads by an empirically determined factor.

Frictional drag is apportioned to the guide tubes and to the fuel rods on the basis of fraction of total wetted perimeter adjacent to a given flow channel or subchannel. The only form losses present are due to spacer grids. These losses are applied completely to the guide tubes, as the spacer grids are welded to the guide tubes. A portion of these losses is ultimately transmitted to the fuel rods through sliding friction; however, this effect is accounted for later via friction elements in the CESHOCK structural mode [14].

For the end fittings, a solid plus fluid control volume is used. Therefore, end fitting drag loads are not explicitly calculated by summing contributions due to pressure, gravity, fluid inertia, and fluid momentum effects.

2.3.2 Detailed Non-Linear Internals Models

Detailed structural models were developed. These mathematical models consisted of lumped masses connected by bar or beam elements which represented the elastic properties of the actual structures. The methods used to develop these models followed the procedures described in CENPD-42 [13] and, in addition, included a more detailed representation of the interfaces between the core support barrel, upper guide structure, and reactor vessel. Hydrodynamic coupling effects caused by the water on either side of the core support barrel were also computed. These coupling terms were calculated as a function of the structural geometry and boundary conditions.

Detailed lateral structural models were developed using the Calvert Cliffs reactor internals. The Calvert Cliffs model is used as a generic model and is being used to represent the St. Lucie internals because of geometrical similarities (other than the thermal shield). This approach will result in conservative loads for St. Lucie 1 since the results presented in Reference 13 show that the presence of a thermal shield reduces the lateral LOCA loadings. The detailed lateral generic model is shown in Figure 8 and the nodal locations are presented in Table 8.

In the axial direction, a detailed model was also developed for the Calvert Cliffs reactor internals. The Calvert Cliffs axial model is conservatively representative of the St. Lucie internals, since Reference 13 indicates that the presence of a thermal shield slightly reduces the vertical responses. Figure 9 and Table 9 show the vertical model.

The computer program, CESHOCK [14] is used to determine the dynamic responses of the models when subjected to LOCA excitation. The program solves the differential equations of motion for lumped parameter systems using a direct step-by-step numerical integration procedure. The displacement, velocity and acceleration of each mass are determined as a function of time. In addition, the member developed loads in all of the couplings are calculated at each timestep and the maximum displacements and forces are summarized for each problem.

2.3.2.1 Horizontal Models and Loads

For the plant, the model for the horizontal direction was developed using the beam elements to represent the lateral stiffness between mass points. Flexible components such as the fuel assemblies and the CEA shrouds were modelled in greater spatial detail than those representing more rigid structures such as the pressure vessel to assure accurate structural responses. The lumped mass model represents the continuous distribution of mass and stiffness exhibited by the actual structure. Rotary inertias are included to properly account for angular accelerations.

Finite element models were used to compute the stiffnesses of complex components such as the core support barrel and upper and lower flanges. Non-Linear springs were used to represent impacting between various components. A.

non-linear rotational spring between the upper guide structure support plate and the fuel alignment plate represents the rotational restraint exerted by the control element assembly shrouds.

The core support barrel upper region was modelled in detail to represent the possible interactions between the CSB upper flange, UGS support plate and the pressure vessel ledge. Linear, non-linear, hysteresis and friction couplings represent this complex interface region. Rotational springs exhibiting bi-linear moment-rotation characteristics are used to calculate the relative rotation between the upper flanges which are held together by the holddown ring.

Non-linear gap springs represent possible impacting between the pressure vessel ledge, the CSB upper flange and upper guide structure support plate (UGSSP), and between the CSB cylinder and the UGS cylinder. Hysteresis couplings account for the shear resistance of the alignment keys to relative translational motion between the upper region components and friction elements represent the resistance forces developed by the holddown ring preload. The four types of couplings described above model the complex interactions that may occur in the interface region during a LOCA. The reactor core is represented in detail in the lateral internals model to account for feedback effects on core plate motion. Nodes are located at each spacer grid in each of the five columns of fuel which represent the entire core. Non-linear couplings are used on the peripheral bundles to represent the effects of spacer grid impacting.

Hydrodynamic mass effects are included for the components in the reactor system. The effect of water in the core barrel/water vessel annulus is accounted for by computing hydrodynamic coupling terms based on the structural geometry and boundary conditions. Hydrodynamic masses are computed for all other components in the system and directly combined with structural masses.

The CEA shrouds are combined into four groupings determined from test results. These groupings are selected on the bases of similarity in lateral cross-flow load distribution.

During a cold leg break LOCA, a rarefaction wave initially propagates downward in the annulus between the core support barrel and reactor vessel. This sudden depressurization causes the pressures in the circumferential direction to vary asymmetrically with time. For this reason, a set of horizontal axes both parallel and perpendicular to the hot leg nozzles centerline are chosen to represent the two-dimensional state of lateral LOCA loadings.

For the calculation of lateral direction cold leg break LOCA loads, a Fourier decomposition of the asymmetric pressure distribution is first performed. Of these coefficients, only the sine and cosine components result in a beam type loading. These coefficients are then integrated over the surface area of the core support barrel to obtain the dynamic LOCA forcing function. Figures 10 and 11 show the total core support barrel loads acting in two perpendicular directions for the generic plant. These loads are computed on the basis of a full break using the model and methodology described in Section 2.1.3 and

Reference 19. As previously stated, the break in St. Lucie is physically limited in extent. The loads acting across the barrel in St. Lucie for the limited break are approximately 60 percent less as shown in Figures 12 and 13.

A hot leg break produces lateral cross-flow loads which act on the control elements assemblies. These loads act in a direction parallel to the axis of the hot legs and depend on the transverse pressure differentials and drag effects. The total cross-flow loads for the St. Lucie 1 plant are shown in Figure 14.

During the development of the generic plant horizontal model, several different friction coefficients were used with constant normal forces in the core support barrel upper flange interface region in order to determine the effects on the internals responses. The chosen bounding case coefficients were selected for stainless steel sliding on stainless steel. The lower bound represented the generic plant baseline case using nominal values and the upper bound included larger but justifiable values. Normal forces resulting from the steady state loads on the internals were used in these studies and the results indicated that many of the maximum loads were reduced in the upper bound case.

Since the bending moments, or in effect, the normal forces vary with the amount of relative rotation between the various surfaces, average preloads were determined from the bounding cases. In order to calculate these values, average resultant moments were first determined for each bounding case from a vector summation of the moments from the horizontal response analyses which were performed in directions parallel and perpendicular to the hot legs. The average values of normal forces were then determined from the sinusoidal force distributions produced by the bending moments.

The above procedure was only used to calculate normal forces between the core support barrel flange and reactor vessel ledge, the core support barrel flange and upper guide structure flange, and between the upper guide structure flange and the reactor vessel for the generic plant. Average values of normal forces were computed from the hot and cold leg break baseline cases. The results indicated that only the average normal force between the core support barrel and the reactor vessel increased from the values used in the baseline case.

Additional horizontal response analyses were performed using the above revised values of normal forces with nominal values of static and dynamic friction coefficients. These increased friction cases were used to determine factors which were defined as the ratios of loads calculated in the nominal friction case and the baseline case. The results for the generic plant applicable as bounding for St. Lucie 1 are presented in Section 3.7 for the internals and in Section 3.8 for the fuel.

2.3.2.2 Vertical Models and Loads

The vertical model stiffness values were calculated using bar elements for most of the model members. Finite element analyses were employed for computing the stiffnesses of the flanges, upper guide structure, and lower support

structure. Non-linear couplings were included to account for such effects as friction between the fuel rods and guide tubes, and impacting between the various structural components.

The core support barrel upper region was modelled in detail to represent the interaction between the core support barrel and upper guide structure flanges with the pressure vessel ledge. The preloaded expansion compensating ring was modelled as a non-linear member which allows the flanges to separate until the ring is flattened. The axial members connecting the UGS flange, and pressure vessel ledge were modelled with compression only springs. Finite element analyses were used to compute the non-linear stiffnesses of the core support barrel and upper guide structure flanges which depend on the direction of loading.

Additional spatial detail was added in the fuel region to accurately compute the dynamic response of the fuel with the adjacent plates. The guide tubes were modelled using the non-linear material properties of the zircaloy stress-strain curve. Friction elements were used to represent the sliding interactions between the fuel rods and spacer grids. Non-linear members were also used to represent the compressive stiffnesses of the lower end fittings which can only develop compressive loads against the core support plate. The upper end fitting was also modelled as a non-linear member and accounts for the steady state preload forces exerted on the fuel and the changes in preload as the fuel moves relative to the fuel alignment plate.

The applied LOCA loads were calculated using a control volume formulation. In this method, the internals structure and contained water are sectioned into solid plus fluid control volumes. Across each volume, the fluid momentum equation is solved as a function of time to compute the LOCA loads. This method accounts for fluid pressure and momentum effects which act on all of the structures within each control volume.

Steady state initial preloads and static deflections were also calculated for these detailed axial models. These preloads are the result of structural weights, holddowns, and normal operating flow forces. Without these values, the model would not be initially at rest.

2.3.3 Reduced Internals Models

Reduced three-dimensional models of the St. Lucie reactor internals were developed from the detailed internals models for incorporation into the reactor coolant system as shown in Figures 3(a) and 3(b). The purpose of these condensed internals models is to account for the effects of the interaction between the internals and the vessel. They are not intended to be used in the calculation of internals responses. The reduced internals models are compatible with the reactor coolant system model and the computer programs utilized in the analysis of the coolant system.

The reduced internals models were developed to produce reactor vessel support loadings equivalent to those obtained from the detailed internals models in both the vertical and horizontal directions.

Figure 15 shows the generic plant reduced internal model, which is nearly identical to that used in St. Lucie to evaluate the vessel supports adequacy.

2.3.4 Core Support Barrel Shell Models

Separate finite element models of the core support barrel are developed for response analyses following both the hot and cold leg breaks. For the cold leg break a dynamic response analysis is performed because of the asymmetric nature of the resultant applied loadings on the barrel. Conversely, the hot leg break results in uniform, axially varying compressive loads on the barrel and its response to these loads is determined through stability analysis.

2.3.4.1 Shell Vibration Model (Cold Leg)

The core support barrel was modelled in detail using a finite element representation. Thin conical shells of revolution joined at their nodal point circles were used as elements. The length of each element was a fraction of the shell attenuation length and, at areas of structural discontinuity, where rapid changes in the stress function occur, the nodal points were more closely spaced. The results of the generic analysis are used to conservatively assess the structural integrity of the St. Lucie core support barrel since it has been shown in Reference 13 that the presence of a thermal shield reduces the intensity of the LOCA loads acting on the barrel, and since the break for the generic analysis is larger than the physically possible break area of St. Lucie.

Several boundary conditions are imposed on the finite element models to simulate the proper restraints. At the upper flange, motion is restricted in the axial, radial, and tangential directions. The CSB lower flange is restricted from moving in the hoop direction by the lower support structure and the snubbers prevent the adjacent elements from displacing in the tangential direction. In addition, the effect of the weight of the internals components resting on the lower flange is considered by increasing the mass density of the flange. The finite element model is shown in Figure 16.

2.3.4.2 Shell Dynamic Stability Model

A finite element model of the core support barrel shown in Figure 17 was formulated for use in the shell stability analysis. The model and the results of the generic analyses are assumed to conservatively apply to the St. Lucie 1 plant.

The core support barrel model consisted of a series of cylindrical shell elements joined at their nodal point circles and included detailed representations of the upper and lower flanges. The length of each element was a fraction of the shell attenuation length and the nodal points were more closely spaced at areas of structural discontinuities. Due to the symmetric nature of the hot leg break applied loadings, the core support barrel shell model was subjected to uniform pressure differentials which were assumed to vary linearly in the axial direction. Since the barrel upper flange is constrained against vertical motion by the reactor vessel ledge, upper guide structure flange, and the hold-down ring, an axial restraint was imposed to prevent motion in this direction.

2.3.5 Internals Response Analyses

The dynamic responses of the reactor internals to the postulated pipe breaks were determined using the various models described in the previous sections. Horizontal and vertical analyses were performed for both the hot and cold leg breaks to determine the lateral and axial beam mode responses of the reactor internals to the simultaneous LOCA forces and reactor vessel motion excitation. Shell response analyses of the core support barrel were also performed for both breaks to obtain the shell mode contributions to the barrel stresses. Each of the above analyses were performed for the generic plant as conservatively applicable to St. Lucie 1.

2.3.5.1 Inlet (Cold Leg) Break Analysis

The postulated cold leg break results in simultaneous vertical and horizontal beam and shell mode excitation. The horizontal and axial responses to these excitations were calculated for the generic plant, using the methods described below. The results of the generic plant internals horizontal responses can be conservatively applied to St. Lucie 1 since the presence of a thermal shield has been shown to reduce the responses. Shell response analyses of the core support barrels were also performed to obtain the shell mode contributions of the components.

2.3.5.1.1 Horizontal Response

The dynamic time history responses of the reactor internals to the horizontal loads resulting from the cold leg break were determined with the CESHOCK code. The input to these analyses were the core support barrel force time history and the reactor vessel motion time history which was determined using the reduced internals models in the reactor coolant system analyses. These motions were calculated at the reactor vessel ledge and snubber elevations.

The horizontal response analyses were performed in directions both parallel and perpendicular to the hot legs because of the asymmetric nature of the applied loadings. The results of these analyses were time dependent member loads and nodal displacements, velocities and accelerations in both directions. Time phased combined loadings were computed for all of the linear members. For the non-linear members such as the snubbers and core shroud guide lugs, the maximum tangential loadings were used. In addition, the core support plate, core shroud, and fuel alignment plate displacement time histories were saved as input to the detailed core model.

These loads were later compared to those presented in CENPD-42. The loads were compared in the vertical direction and with the resultant of the horizontal directions. Conservatively calculated component stresses using the combined maximum lateral and axial loads were computed if the loads in a given direction exceeded any of the previously calculated values.

Time phased combined axial and horizontal loads were used to reduce conservatism whenever any of the conservatively calculated component stresses from the set of maximum loads exceeded the ASME code allowables. Since the maximum horizontal and axial loads occurred at different times and resulted in different component stresses, several calculations were made and the "worst cases" were compared to the allowables. A further description of this procedure and the results are presented in Section 3.7.

In order to determine the total core support barrel stresses, the beam mode loadings (CESHOCK results) were combined with the shell mode loadings (ASHSD results) at the times of peak loadings. The ASHSD results consisted of shell forces, moments, and stresses as a function of time for each element in the model. These combinations included the maximum generic plant axial internals response loads from the CESHOCK analysis. Several time points were investigated in order to determine the most conservative stresses and stress intensities. Time phased load combinations were also used to reduce the conservatism. Stress analyses using these methods were performed for the generic plant. The results of the generic plant assessment are conservatively applied to the St. Lucie 1 plant which has a thermal shield. This method of combining loads more accurately represents the dynamic effects of the internals and fuel on the beam response of the core support barrel.

2.3.5.1.2 Vertical Response

A detailed vertical response analysis was performed only for the generic plant following the cold leg break. This approach resulted in internals and fuel loads which are conservative for St. Lucie 1 because of the presence of the thermal shield.

In this analysis, the internals model was subjected to LOCA forces and reactor vessel motions obtained from the reactor coolant system analysis using the generic plant reduced internals model. The CESHOCK code was used to perform the axial response analysis and the results considted of maximum member loads and nodal displacements, velocities, and accelerations. These loads were compared to the values previously calculated in CENPD-42 for St. Lucie 1.

Whenever any of the new axial loads exceeded the previous values, component stresses were calculated using the maximum axial and combined horizontal loads. Time phased load combinations were used to reduce the stresses whenever the conservatively calculated stresses based on the maximum load combination resulted in values which exceeded the ASME code allowable. A further description of the procedures used and the final results are presented in section 3.7.

The generic plant detailed axial response analysis also provided detailed fuel assembly loads and deflections. The maximum developed fuel bundle and fitting loads were later used in the detailed stress analyses of the fuel rods and guide tubes for the generic plant. The generic plant axial fuel bundle responses were conservatively assumed to be applicable to the St. Lucie 1 plant.

2.3.5.1.3 Shell Vibration Response (Cold Leg)

A cold leg break will cause the pressure transients to vary both circumferentially and axially. During the calculation of the blowdown loads, these pressures are computed at several equally spaced circumferential locations and at several axial elevations. In order to compute the core support barrel asymmetric LOCA loads, a Fourier decomposition of the pressures is performed at each axial station. A linear distribution is assumed between axial stations. The resulting pressure coefficients are then integrated over the surface area of the barrel to obtain the dynamic LOCA loads.

The dynamic responses of the generic plant core support barrel shell model following the cold leg break with the beam loadings ($\sin\theta$, $\cos\theta$) removed were determined by the ASHSD computer code [15]. The code is applicable to axisymmetric structures of arbitrary shape subjected to asymmetric static or dynamic loads. The ASHSD code considers each load harmonic (Fourier term) separately and superimposes the response of each barrel harmonic to obtain the total response. The output of the ASHSD code consists of nodal displacements, resultant shell forces and shell stresses as a function of time.

The maximum displacements, forces, and stresses were later computed for the barrel using the results from ASHSD. The results of the generic analysis were conservatively assumed to be applicable to the St. Lucie 1 barrel because of geometric similarities and the fact that the presence of the thermal shield reduces the intensity of the LOCA loads. The maximum loads obtained from these analyses were combined with the horizontal and vertical CESHOCK core support barrel response loads in order to obtain the resulting conservatively calculated stresses and stress intensities. Time phased load combinations were also used wherever any of the ASME code allowables were exceeded.

2.3.5.2 Outlet (Hot Leg) Break Analysis

Horizontal and vertical nonlinear internals and core support barrel shell response analyses were performed for the hot leg break. The generic plant results were conservatively applied to the St. Lucie 1 internals. In addition, a single core support barrel shell dynamic stability response analysis was performed for the generic plant core support barrel and the results were conservatively applied to the St. Lucie 1 plant specific core support barrel.

2.3.5.2.1 Horizontal Response

The dynamic time history responses of the generic plant, representing St. Lucie 1 reactor internals, to the horizontal loads resulting from the hot leg break were determined with the CESHOCK code. Input to these analyses were the control element assembly shroud crossflow forces and the reactor vessel motion time history determined from the generic plant reactor coolant system analysis. The forces consider pressure differentials and drag contributions which depend on the different locations and geometries. Due to the symmetric nature of the pressure differentials around the core support barrel, the transverse forces on the barrel and other internals were negligible.

The response analyses were performed only in the direction parallel to the hot legs. The results consisted of the maximum time dependent member loads and nodal displacements, velocities, and accelerations. These loads were compared to those presented in CENPD42 for St. Lucie 1. Whenever any of the new loads exceeded the previously calculated values, detailed combined load stress analyses were performed using the maximum axial loads from the generic plant vertical response analysis. Time phased combinations were also used to reduce the conservatism whenever the above procedure resulted in calculated stresses which exceeded the ASME code allowables. The results of the analyses and a further description of the procedures used are presented in Section 3.7.

2.3.5.2.2 Vertical Response

A single vertical response analysis was performed. The methods used in Section 2.3.5.1.2 are applicable to both the hot and cold leg breaks.

2.3.5.2.3 Shell Dynamic Stability Response

The SAMMSOR/DYNASOR code [16,17] was used to determine the buckling potential of the generic plant core support barrel following a hot leg break. The SAMMSOR portion of the code was used to generate the mass and stiffness matrices for the shell, and the DYNASOR portion of the code calculated the dynamic response using the Houbolt numerical procedure.

The analyses were performed for the second, third, and fourth cosine harmonics using the maximum values of as-built initial imperfections for the generic plant. In these analyses, the applied transient loads were circumferentially uniform but varied linearly in the axial direction. Overload analyses using factors of 1.33, 2.0, and 4.0 were also performed to determine the buckling potential of the barrel. The resulting maximum radial displacements were linear and were therefore well within the ASME code requirements for dynamic stability. The results of this analysis can be conservatively applied to the St. Lucie 1 plant because the presence of a thermal shield reduces the core support barrel loads [13]. In addition, the low level of load input magnitude and the results of the analysis indicate that all of the responses are far removed from stability considerations.

2.4 Fuel

2.4.1 Combustion Engineering Fuel Assembly Description

The Combustion Engineering 14x14 fuel assembly consists of 176 fuel rods, five control element guide tubes, one Inconel and eight Zircalloy fuel spacer grids, a lower end fitting, and an upper end fitting which incorporates a holddown device. The guide tubes, spacer grids and end fittings form the structural frame of the fuel assembly.

The lower end fitting consists of four posts and a flow plate, fabricated as a single stainless steel casting. The posts are designed to receive the alignment pins of the core support plate and thereby provide positive lateral locating of the lower end of the fuel assembly. The flow plate consists of an open lattice-work of interconnecting ribs which permit the coolant flow to enter the fuel assembly and at the same time provide bottom support for the fuel and poison rods. Portions of the lower end fitting are machined to accept the guide tube lower ends and the flow skirt of the Inconel grid.

The upper end fitting assembly consists of two case CF-8 stainless steel plates, five 304 stainless steel machined posts, and five helical Inconel X-750 springs. The upper end fitting assembly attaches to the guide tubes and has features which provide for grappling of the fuel assembly, locating the top end of the fuel assembly laterally, and a holddown capability.

The lower cast plate is similar to the plate of the lower end fitting in that it also has an open lattice-work of interconnecting ribs which permits coolant flow to leave the fuel assembly with little restriction. The plate has four machined holes which receive the outer posts and a threaded center hole to receive the center post.

The upper cast plate consists of four arms connected by a central ring and has features which permit positive grappling during fuel handling. Both the arms and the central ring are machined to permit free passage of the plate over the interfacing post surfaces.

The four outer posts of the upper end fitting mate with holes in the fuel alignment plate to locate the upper end of the fuel assembly. The center post is threaded into the lower cast plate of the upper end fitting and locked in place by welding.

The upper end fitting is assembled to the fuel assembly by the four outer posts which are threaded into the mating portion of the outer guide tubes. When assembled, the upper cast plate of the upper end fitting is preloaded by the springs which surround each post.

The outer guide tubes are Zircalloy-4 and are fabricated by welding a fitting to each end. The lower threaded portion mates with the lower end fitting. The upper threaded portion provides a means by which the upper end fitting may be assembled to the guide tubes. The center guide tube, also of Zircalloy-4, is of one piece construction.

The guide tubes provide a path for the control element assembly fingers, house in-core instrumentation and neutron sources, provide a deceleration zone for scramming control element assemblies, and provide a basic frame to which the grids are assembled and welded in place. The subassembly of grids and the lower end fitting form what is called a grid cage and when coupled with the upper end fitting form the basic structural frame of the fuel assembly.

The fuel rod spacer grids are fabricated from performed Zircalloy or Inconel strips (the lower spacer grid material is Inconel), interlocked in an egg crate fashion, and welded together. The spacer grids maintain the fuel rod pitch over the full length of the fuel rods by providing positive lateral restraint. The fuel rods are restrained from axial motion by the frictional forces developed by the spacer grid leaf springs. Each cell of the spacer grid contains two leaf springs and four arches. Each leaf spring presses the fuel rod against two arches, thereby restricting relative motion between the grids and the fuel rods. The spring and arch positions are reversed from grid to grid to provide additional restriction to relative motion. The perimeter strips which surroung the egg crate construction also contains springs and arches in addition to features which prevent hangup of grids during fuel handling.

The eight Zircalloy-4 spacer grids are fastened to the Zircalloy-4 guide tubes by welding. Each grid is welded to each guide tube at eight locations, four on the upper face of the grid and four on the lower face of the brid, where the spacer strips contact the guide tube surface. The lowest spacer grid (Inconel) is not welded to the guide tubes because of material differences. The perimeter strip of the Inconel grid is welded to the perimeter of the lower end fitting.

The fuel rods consist of UO_2 pellets, a compression spring, and spacer discs, all encapsulated within a Zircalloy-4 tube which is welded into a hermetic enclosure. The fuel cladding is slightly cold worked Zircalloy-4 tubing.

The Calvert Cliffs 1 and 2 (generic plant) and St. Lucie 1 fuel assemblies are identical.

2.4.2 Fuel Testing

Tests were conducted on 14 x 14 fuel assembly components representative of the St. Lucie plant. The discussion below outlines each test and presents some of the actual test data.

2.4.2.1 Static Load-Deflection Tests

For the lateral load-deflection tests, the full-size fuel assembly was mounted in the seismic test stand and withdrawn laterally in specified increments. Measurements include: lateral load, lateral deflection at several spacer grids, and guide tube strain at several locations. Additional measurements were made which allowed calculation of the stiffness of the spacer grid/guide tube joint. A schematic of the test set-up is shown in Figure 18.

A typical load-deflection curve is shown in Figure A-1 of Appendix A. Fuel Assembly lateral stiffness and hysteretic response were established by this data. At each increment of lateral load, strain and guide tube-spacer grid rotation measurements were made.

2.4.2.2 Fuel Bundle Dynamic Tests

For the lateral fuel assembly impact test, the bundle was mounted in the same test stand used for the load-deflection test. The bundle was withdrawn a specified distance, released, and allowed to strike a plate which simulated the core shroud. The dynamic response of the bundle was monitored by measurement of displacement vs. time at three (3) spacer grid locations and velocity vs. time at the central spacer grid. A load cell recorded impact load at the central spacer grid. This test was performed in air and water environments in order that water effects might be evaluated. A schematic of the test set-up is shown in Figure 20.

Figure A-2 in Appendix A shows typical impact load data.

Figures A-3 and A-4 of Appendix A show typical data on fundamental frequency and damping ratio for the free vibration decay. (These data were taken on the above test fixture with the impact plate removed so that no impacting occurred.)

2.4.2.3 Spacer Grid Impact Test

For the spacer grid impact tests, a fuel assembly section consisting of a spacer grid with guide tubes and fuel rods corresponding to one spacer grid span was mounted in a test fixture. With this fixture, the entire fuel assembly section could be dropped from a specified height and allowed to strike an impact surface, or a weight could be dropped and allowed to impact on the spacer grid. From these tests, spacer grid dynamic characteristics and structural strength were determined. In addition, the fuel assembly section drop tests were performed in water to establish fluid cushioning behavior during impact.

The air "weight drop" test was used to determine grid strength when a through grid load is applied. This loading is representative of a bundle being simultaneously loaded from both sides. The fuel section drop test was used to determine grid strength when a one-sided load is applied. This loading is representative of a free bundle impacting against another bundle or the core shroud. For both of these tests, drop height was incrementally increased until the grid strength was established. The cold grid strengths determined for through-grid and one-sided loads are shown in Table A-1 of Appendix A.

The drop tests in water were conducted with flow restriction plates that simulated fluid effects for the in-reactor geometry. Figure A-5 shows typical data from this test.

2.4.3 Fuel Analysis Models

Detailed structural lumped mass-spring models of the fuel assemblies were developed based on a correlation with static and dynamic test results. These models were analyzed for both hot and cold leg breaks with the CESHOCK Code [14]. The resulting component loads and displacements were used to determine fuel assembly stresses and spacer grid impact loads. A beam column model of a full assembly has also been developed for use in an analysis of simultaneous compressional and lateral loading.

2.4.3.1 Horizontal Model

A generic horizontal fuel assembly model has been developed for Calvert Cliffs and thus St. Lucie 1 from correlation studies with test data. The model is used to represent the entire core in the detailed internals model and a single row of fuel assemblies in the fuel analysis model. The detailed core model is excited by applying the fuel alignment plate, core shroud and core support plate motions obtained from the detailed internals models with pipe rupture loads and vessel motions considered. These motions are larger for the generic plant with its full break for cold leg, than for St. Lucie 1, which has a limited cold leg break opening area.

The lateral fuel assembly model was developed to exhibit a dynamic response similar to that of the test bundle. The fuel assembly was modelled with a constant flexural rigidity and a rotational spring at each end. The magnitude of the bending stiffness and torsional spring constants were obtained from a correlation of static deflection test data in conjunction with observed fundamental frequencies derived from the pluck vibration tests of the bundle in air. The added mass coefficients for the fuel assembly were determined from the pluck vibration tests in water.

The detailed fuel model includes non-linear elements which represent the possible impact between adjacent fuel assemblies and the core shroud. The magnitude of the impact stiffness was derived from correlation with pluck impact test results. Also, the grid strengths and coefficient of restitution were determined from the spacer grid drop tests in air.

2.4.3.2 Vertical Model

A vertical fuel assembly model is developed from correlation with static stiffness and drop tests and will be also included in the detailed internals (Figure 9
model. The model includes non-linear couplings to represent the end fittings and separate parallel branches representing the grid cages and fuel rod. Friction elements are used to represent stick-slip motion between the fuel rods and spacer grids.

The model was subjected to both LOCA and drag loads which were computed with the control volume method utilizing an integrated fluid momentum equation. The drag loads were composed of both frictional and spacer grid form drag. Frictional drag was apportioned to both the fuel rods and guide tubes and was calculated using friction factor which was dependent on the flow channel equivalent diameter, cross-sectional area, fluid flow rates and densities. The form drag was calculated using an experimentally determined loss factor correlation as a function of Reynolds Number. In addition, crud effects were accounted for by multiplying the drag loads by an empirically determined factor.

2.4.3.3 Dynamic Beam-Column Model

A detailed mathematical model of the generic plant fuel assembly was developed based on correlation with static and dynamic test results. The test results included lateral static stiffness, pluck vibration and spacer grid impact data. The guide tubes and upper and lower end fittings were modelled with two-dimensional beam elements. The fuel rods were modelled with a series of spar elements such that vertical sliding forces between the fuel rods and spacer grids and impact forces between the fuel rods and flow plates are accounted for in the model. The flexural rigidity of the fuel assembly is included in the structural properties of the guide tube and end fitting members. These members form the grid cage space frame which supports the fuel rod arrays.

At locations where gaps may occur (e.g., fuel rod/lower end fitting flow plate interface) spring/gap elements acting in the direction normal to the impact surface are used to represent its dynamic characteristics. The beam-column fuel assembly model was used in a dynamic response/stability analysis of simultaneous axial and lateral LOCA loading.

Hydrodynamic mass effects are modelled via dynamic fluid coupling elements between the guide tube nodes and a fixed point of reference. The fluid coupling element modifies the structural mass matrix. The properties of the fluid coupling element were selected to yield a beam-column model fundamental natural frequency in the lateral direction equivalent to that obtained from free vibration test data in water.

The dynamic characteristics of the beam column model in the vertical direction are verified by comparing its calculated natural frequencies to those obtained via theoretical eigenvalue analysis of the fuel assembly components.

Effects of adjacent structures in both the lateral and vertical directions were included in the beam-column model. Structural members between the subject peripheral fuel assembly (results of Section 2.4.4.1 demonstrate the peak lateral response to occur in the peripheral assembly) and the adjacent fuel assembly or core shroud represent the appropriate impact stiffness and initial nominal gap. Interface between the fuel assembly and core support plate (CSP) or fuel alignment plate (FAP) is represented by rotational spring and spring/gap elements. However, vertical analyses described in Section 2.4.4.1

indicate the linear holddown springs located between the FAP and fuel assembly to be active throughout the dynamic response history. Therefore, only a linear member is required at this location to model the interface between the fuel assembly and FAP.

2.4.4 Fuel Response Analysis

The detailed horizontal core models consisting of the longest row of fuel assemblies across the core were analyzed for both hot and cold leg breaks. The CESHOCK Code was used to perform these analyses which were done in directions both parallel and perpendicular to the hot legs following the cold leg break and parallel to the hot leg for the hot leg break. The results of these analyses included spacer grid impact loads and component loads and displacements which were later used in the fuel assembly stress evaluation. The procedures used and the results of the fuel evaluation are presented in Section 3.8 of Appendix A.

2.4.4.1 Inlet Break Analysis

Detailed lateral response analyses for a cold leg break were performed using CESHOCK for the generic plant representing St. Lucie 1. The input excitation was the core support plate, fuel alignment plate, and core shroud displacement time histories which were calculated from the detailed internals response analyses. The results of the analyses were the maximum fuel bundle moments, shears, and displacements and the maximum one-sided spacer grid loads. The maximum through grid or the steady state components of loading acting simultaneously on both sides of the grids were also calculated. These results were later used to perform a stress evaluation of the fuel.

2.4.4.2 Outlet Break Analysis

Lateral response analyses for a hot leg were performed in the direction parallel to the hot legs using the detailed fuel models. The methods, described in Section 2.4.4.1 are directly applicable to the hot leg breaks.

2.4.4.3 Dynamic Beam-Column Analysis

The dynamic beam-column analysis determined any additional bending stress and stability of the fuel assembly due to concurrent lateral and axial loading. The response included interaction with other structural components in the lateral and vertical direction. The detailed beam-column model was developed to be consistent with the general purpose finite element code ANSYS[20]. By employing the large deformation option, deflection under load was used to continuously redefine the structural geometry, thus producing a revised stiffness matrix.

The starting time of the dynamic beam-column analysis was selected to include regions of the LOCA response history during which peak lateral loads, co-excited with significant axial loads. Results of the analyses presented in Sections 2.4.4.1 and 2.4.4.2 indicated that the peak fuel assembly responses in separate lateral and axial directions occurred during a full power inlet break in the Z-direction. The peak axial responses occurred at approximately 100 msec. Preliminary beam-column analyses have shown that beam-column effects are more sensitive to lateral bending moments than to axial forces. Therefore, the critical time range, with respect to beam-column effects is 180 to 200 msec. A 170 msec. start time was selected and the detailed beam-column analysis was performed to 210 msec.

Initial conditions obtained from the separate axial and lateral analyses at 170 msec. were applied to the beam-column model. Axial displacements and velocities at 170 msec. were applied to the model at guide tube, fuel rods, core support plate and fuel alignment plate node locations. In addition, axial LOCA and drag loads were applied to the guide tubes and fuel rods. In the lateral direction displacements, rotations, velocities and angular velocities were applied at guide tube, core support plate, and fuel alignment plate node locations. In addition, the lateral displacements and velocities of the nodes representing the adjacent fuel assembly and core shroud were defined at 170 msec.

Loading time histories were specified from 170 msec. to 210 msec. These consisted of axial LOCA and drag loads on the guide tubes and fuel rods; displacements (in both axial and horizontal directions) at the core support plate and fuel alignment plate; rotations at the core support plate and fuel alighment plate and lateral displacements of the nodes representing the adjacent fuel assembly and core shroud. Therefore, the beam-column analysis accounted for all interactions between the subject fuel assembly and the remainder of the reactor internal components in the lateral and axial direction.

The results of the analysis included transverse shears, moments, axial loads, and nodal displacements as a function of time. These results were later used to perform a stress analysis of the fuel assembly. The results of this analysis indicate that the beam-column effect does not significantly increase the maximum fuel bundle stresses.

2.4.5 Faulted Condition Criteria for Fuel Assembly Evaluation

The basic functional requirement which must be satisfied by the fuel assembly during the event is that the structural components of the assembly (end fittings, guide tubes and grids) must be capable of maintaining the fuel rods in a coolable array when subjected to the mechanical loads predicted to result from the occurrence of the event.

In order to permit analytical determination of the capability of the fuel assembly to satisfy the above functional requirement, specific quantitative

criteria are established for each structural component in the fuel assembly. These specific criteria (listed by component) are discussed in the following sections.

2.4.5.1. Upper and Lower End Fitting Castings

The end fitting castings are made from 304 stainless steel, Grade CF-8. The adequacy of these components to withstand the mechanical loads is determined by calculating the stress intensities resulting from loads and comparing the calculated stress intensities with limits defined by:

a) The primary membrane stress intensity, P_m, must not exceed 2.4 S_m, where S_m is the design stress intensity value for nominal conditions and is equal to 10,500 psi. Therefore, the maximum allowable primary membrane stress intensity is equal to 2.4 x 10,500 or 25,200 psi.

b) The sum of the primary membrane stress intensity, P_m, and the primary bending stress intensity, P_b, must not exceed the product of 2.4 S_m and a section factor, F_s, which depends on the cross-section over which the bending moment acts.

2.4.5.2 Upper End Fitting Posts

The five upper end fitting posts are made from wrought 304 stainless steel. The performance of these components is evaluated in exactly the same way as that of the end fitting castings discussed above, except that the difference between properties of wrought and cast 304 stainless steel results in a slightly higher design stress intensity (S_m = 12,000 psi) for the posts than for the castings.

2.4.5.3 Upper End Fitting Holddown Springs

The upper end fitting springs are fabricated from Inconel X-750 wire. The performance of these components is evaluated by calculating the shear stress resulting from the spring being compressed to its solid height. This calculated shear stress must not exceed the yield strength in shear for this material. This maximum allowable shear stress is equal to 99,000 psi.

2.4.5.4 Guide Tubes

There are no specific stress criteria applied to the evaluation of fuel assembly guide tubes for the large break LOCA anlaysis, for the following reasons:

a) Control rod scram is not a requirement.

b) The existance of the fuel rod coolable array is dependent upon the spacer grid performance during the event. Minor distortions of the guide tubes will not affect the assembly inlet or outlet flow conditions (controlled by the end fittings) nor the individual flow channel conditions (controlled by the spacer grids).

2.4.5.5 Spacer Grids

The spacer grids are the primary factor in assuring that fuel rods remain in a coolable array. The capability of the grids to perform this function is determined by comparing the predicted lateral impact loads associated with the postulated event to the lateral crush strength of the spacer grid, which was determined by test. Resulting values are listed in Table A-1 (room temperature) and Table A-3 (operating temperature).

2.4.5.6 Fuel Rods

It is a requirement the fuel rod cladding be capable of withstanding the loads resulting from the mechanical excitations occurring during the postulated event without failure resulting from excessive primary stresses. Loads resulting from the thermal and differential pressure fluctuations later in the event have been addressed in LOCA analyses previously provided.

The adequacy of the fuel rods to withstand the calculated loads is determined by comparing the calculated stress intensities which result from the axial and lateral loads to allowable stresses defined by the following formulae:

a) The primary membrane stress intensity, P_m, shall not exceed 0.7 times the ultimate tensile strength, S_u.

b) The sum of the primary membrane stress intensity, P_m, and the primary bending stress intensity, P_b, shall not exceed the product of the allowable primary stress intensity (see Part (a) above) and the 1.46 section factor appropriate to the fuel rods.

The stress intensity limits are listed in Appendix A.

2.4.6 Stress Analysis of Fuel

The pipe rupture response analysis model produces results in the form of spacer grid impact load, axial and lateral loads on the fuel end fittings, and lateral deflected shapes for the fuel assembly. These results are then applied to the analysis of the fuel assembly in the following manner.

- Calculated spacer grid impact loads are compared directly to the experimentally determined load/deformation capability of the spacer grids.

- Axial and lateral end fitting loads are applied (analytically) to the appropriate portions of the upper and lower end fittings, and the resultant stresses are calculated using relatively basic strength of materials methods.

- Lateral deflected shapes are inputed directly into a computer model which then makes use of these shapes to calculate the resultant stress intensities in the axial structural members of the fuel assembly and in the fuel rods. Since the fuel assembly response to the LOCA is a dynamic phenomenon, with an essentially infinite number of axial shapes which could be analyzed, it is necessary to be selective in establishing which shapes are likely to correspond to maximum stress conditions. This is accomplished by evaluating all shapes which correspond to either maximum deflection or maximum apparent curvature at each of the axial modes in the pipe rupture response model.

2.5 Control Element Assemblies

The control element assemblies are not required to operate for safe shutdown for the types of breaks considered; i.e., larger than 0.5 square feet. Thus, the important consideration is that they can be shown to remain integral under the applied loads. The critical loads (those resulting in the largest bending moments at the CEA nozzles) result from cold leg breaks. The modelling used and results from the CEA analysis are reported in Section 3.6..

3.0 RESULTS OF THE ANALYSES

3.1 Vessel Supports

The loads calculated for each reactor vessel support by the method outlined in Section 2.1.4 are reported in Table 3 for the break chosen for the analysis; i.e., the 4.0 sq ft cold leg break at the inlet nozzle; for a range of reactor vessel support stiffnesses. This range covers the possible values of the overall stiffness of the individual reactor vessel supports, the real value being somewhere between the two extremes. It is not possible to quantify the stiffness value more precisely since the modelling of the boundary condition representing embedded steel in the biological shield is subject to variation.

In the support analyses however, the higher loads resulting from the use of the highest stiffness, have been utilized. This insures again that the absolute maximum load per support is computed. In reality, lower values are expected.

The capability of the reactor vessel supports is given in Figure 4 and Table 4 respectively for the RPV support pad capability and the weakest link in the steel support/biological shield structure.

Since the capability of the supports exceed the maximum loads computed for the given break, it is concluded that the existing support system is adequate for that break.

As stated in Section 2.1, it is possible that, as a consequence of the broken discharge line rotation about the pump, a larger break area could form within the cavity, up to a maximum of 7.78 sq ft. This larger break area, requiring a proportionately longer time to open, has virtually no effect on thrust and internal asymmetric loads, but would increase the horizontal external asymmetric load by approximately 15-20 percent over that used in the analysis, as explained in Section 2.1.2. The EAL represents approximately 40 percent of the overall load. Hence, a 20 percent increase in this load would result in less than a 10 percent increase in the overall loading. From Table 4 and Figure 4, it can be seen that this increase would be accommodated by the margins existing in the support system.

It is therefore, concluded that the reactor vessel supports can withstand the largest break in the cold leg piping within the cavity.

Since cold leg breaks outside the cavity do not produce EAL loads and since the IAL is virtually unaffected by the area of the break as explained in Section 2.1.3, it is also concluded that the reactor vessel supports are capable of withstanding any load resulting from postulated ruptures outside the cavity.

A detailed analysis of the reactor vessel support loads resulting from hot leg breaks within the cavity has not been performed. The reasons are as follows: the stiffness of the hot leg pipe combined with the steam generator restraining action, results in a break area within the cavity which is smaller than the cold leg break area, hence resulting EAL would be lower than calculated for the cold leg break; although the thrust force initially would be larger, the IAL would not be colinear with thrust and EAL, but would in fact be approximately orthogonal to them. The resultant horizontal loads on the vessel supports therefore, would clearly be smaller.

For instance, the reactions at reactor vessel supports, due to a hot leg break have been compared to the reactions due to a cold leg break for thrust and subcompartment pressure only.

	Horizontal Hot Leg Break (Kips)	Horizontal Cold Leg Break (Kips)
Cold Leg Spt	4270	3270
Hot Leg Spt	0	3275

Although the load on the cold leg support is more severe for a hot leg break than for a cold leg break, when the effects of internal asymmetric loads are added, the cold leg break will govern.

Vertical loads would be of the same order of those experienced as a result of cold leg breaks, and the capacity of the support system to accommodate vertical loads is significantly higher than its horizontal capability. Hence clearly the reactor vessel support system is also capable of withstanding the effects of postulated hot leg breaks inside and outside the reactor cavity.

A similar conclusion had been reached in our August 1977 report. Differences in maximum loads reported herein from those reported in the August 1977 report are two fold. The August 1977 report did not consider internal gaps or gaps between the support pads and the support structure. The August 1977 report condsidered therefore that all loaded supports would be loaded simultaneously and share the load equally. The agreement of the overall loading between the present and the August 1977 results, confirm that the approach taken in 1977 to assess the loads was not unreasonable.

3.2 Other RCS Supports

The only supports on the primary system, other than the vessel supports, are the steam generator supports. Results of the analyses of the loads imposed on these supports from both hot and cold leg breaks in the system in combination with seismic loads, indicated that none of the design loads have been exceeded, with exception of the loads on the four holdown bolts at the vessel end of the steam generator sliding base and the sliding base itself. The computed and design loads are shown in Table 5. Individual examination of the sliding base, the bolts, and bolt anchorages however indicates that all can acceptably withstand the applied loads. It is therefore concluded that the existing supports design is adequate.

3.3 Reactor Coolant Piping

Table 6 reports the elastically calculated pipe rupture and seismic loads on intact reactor coolant piping associated with the broken loop for the worst break, which is the cold leg guillotine break at the vessel safe end. Examination of this table reveals that all loads fall within the allowable loads with the exception of the load at the RCP discharge nozzle, which exceed the allowable by about 13 percent, on an elastic basis.

Since this analysis is predicated on a 4.0 sq ft cold leg break, by the arguments presented in Section3.1, consideration of the largest break that could occur at the vessel safe end; i.e., 7.78 sq ft, requires that an increase in load of less than 10 percent be examined to assess the adequacy of the coolant piping. Such an increase can be readily accommodated at the RCP suction and RV outlet nozzles. The RCP discharge would be more overstressed (on an elastic basis) and the RV inlet would be very slightly overstressed.

Since only the fluid retaining integrity of this coolant piping needs to be maintained during the postulated LOCA, an analysis conducted on an elasto-plastic basis would conclude that this integrity would be maintained at those nozzles. Since the amount of overstressing calculated on an elastic basis is relatively small, a plastic analysis was not considered necessary.

During the performance of this particular analysis it was calculated that the snubbers on the reactor coolant pumps are overstressed. These snubbers are not needed for these events. However their failure could affect the results. Hence, the analysis was repeated by taking no account of the snubbers. Results are also reported in Table 6. As can be clearly seen, the effect of the presence or absence of the snubbers is negligible.

3.4 ECCS and Connected Piping

The stresses computed from the analysis described in Section 2.2.2 are within 10 percent of the allowable, and hence it is concluded that the ECCS piping and other piping connected to the primary loop, is not adversely affected by the postulated event. Figure 5 shows the model used in the analysis.

Table 7 compares the peak computed stresses, which, in this case, include normal and seismic loads to the allowable stresses. Seismic loads have been included since they had already been combined with the normal stresses.

The margin existing between peak stresses calculated on an elastic basis and stresses that would be allowed within an elasto-plastic analysis further indicates that this attached piping would be able to withstand the imposed loads from the 7.78 sq ft larger cold leg guillotine break.

3.5 Seismic Loads

Pursuant to the Staff's request at the January 16, 1980 meeting, Table 1 provides the design seismic loads at the various support points in the Reactor Coolant System.

3.6 Control Element Assemblies

The control element assemblies are not required to operate for safe shutdown after a loss of coolant event resulting from breaks which are larger than 0.5 square feet. However, in order to comply with existing ECCS analyses methods, the integrity of the elements must be maintained and leakage must be prevented.

The capability of the elements to withstand the effects of the design basis pipe break (4.0 ft^2 inlet cold leg) has been evaluated by determining the response of an individual CEDM to the motion of the reactor vessel head previously computed by the system structural analyses described in Section 2.1.4.

Simplistic elastic analyses of a cantilevered beam indicated that elastic level ASME limits would be exceeded for the input motion. Therefore, an elasto-plastic analysis was performed. This analysis was performed by the PLAST program [1]. The displacements of the reactor vessel head computed by the system structural analysis performed specifically for St. Lucie were applied to the base of the CEDM.

Material properties used for the CEDM analysis in the critical nozzle area are shown in Figure 6a. The analysis utilized operating temperature properties. The model used for the CEDM is shown in Figure 6b.

The results of the elasto-plastic analyses of PLAST are bending moments, forces, and strains at selected points in the model, including the nozzle as a function of time.

To assure that the pressure boundary is not violated, the criterion from the ASME Code, Appendix F, that the integrity of the pressure boundary is assured if the applied loads do not exceed 70% of the plastic instability load was used.

The maximum bending moment occurs at the vessel nozzle of the CEDM. The strain limit which to insure that 70% of the plastic instability is not exceeded is conservatively computed to be that resulting from a rotation of the nozzle of 2 percent.

Figures 7a and 7b show the time varying bending moment or orthogonal components computed by the analyses. Figures 7c and 7d show the input displacements to the analyses in the two horizontal orthogonal directions. Figure 7e shows the moment vs. rotation of the nozzle section of St. Lucie 1 as computed using the approach of Gerber [18], who showed excellent comparison between theory and test data. From this figure, the plastic instability bending moment is shown to be approximately 3.5×10^5 in-lb. The maximum applied moment from the vessel motions resulting from a 4.0 sq ft cold leg break is well below 70% of the plastic instability moment, being less than 1.8×10^5 in-lb. The bending moment is proportional to the vessel motions for a given vessel support stiffness. Since the vessel motions computed for the partial 4.0 square foot break and for the full size break are approximately the same in magnitude, the maximum bending

moment will be approximately the same for large enough break sizes, regardless of the break size. Thus, for the largest possible break in St. Lucie 1 (less than full break), the applied bending moment at the nozzle will be approximately 1.8×10^5 in-lb, which is well below 70% of the plastic instability moment.

Figure 21 provides a comparison between the vessel motions computed specifically for St. Lucie 1 for a 4.0 sq ft cold leg break at the vessel inlet nozzle, and those calculated for the generic plant (Calvert Cliffs), for a full 1414 in^2 cold leg break. The latter has been used for the internals and fuel analysis. As seen, the generic plant vessel displacements are actually less than those computed for St. Lucie. It is therefore concluded that the integrity of the CEAS is assured.

Seismic induced bending moments had been computed for the original design. The maximum bending moment was 1.1×10^5 in-lb.

3.7 Reactor Internals

3.7.1 Acceptance Criteria

The acceptance criteria for the reactor internals following a loss of coolant accident (LOCA) is based upon maintaining the core in place and assuring that adequate core cooling is preserved. This can be accomplished if the following criteria are met. For the core support components, the stress intensities must be less than those listed in the ASME Boiler and Pressure Vessel Code, Section III, Division I, Appendix F. Meeting the stress criteria for core support components assures that the core will be held in place during a LOCA. The difference between the ASME Code allowables and the calculated stress intensities is reported as margin. For the internal structures, the component deflections are limited so that the core is held in place, adequate core cooling is preserved, and the resulting loads do not adversely affect the core support components.

The difference between the calculated stress intensity and the allowable stress intensity per the ASME Boiler and Pressure Vessel Code, Appendix F, is reported as margin. The margin was calculated as a percentage using the following equation:

$$\text{Margin} = \frac{(S_{allow} - S_{calc})}{S_{allow}} \times (100\%)$$

where the term S_{calc} is the calculated component stress intensity being evaluated and the term S_{allow} represents the ASME Code allowable stress intensity of $2.4S_m$ for a membrane condition or $3.6S_m$ for a membrane plus bending condition. The reported margin is therefore a measure of the percent of the stress intensity remaining beyond the calculated stress before the ASME Code allowable stress intensity is reached.

3.7.2 Load Comparison

The initial phase of the evaluation consisted of a comparison of the design verification LOCA loads used in the original analysis as reported in CENPD-42[13], and the present asymmetric LOCA loads considering vessel motion. The three components of the load, including the vertical and horizontal shear forces and the horizontal moment, were compared to the original loads to determine if any portion of the load increased. Any area of the reactor internals with a load component higher than the design verification LOCA loads was evaluated by performing a new analysis using the new asymmetric loads.

The results of the load comparison indicated that the only areas of the reactor internals which did not show an increase in loads with the asymmetric load analysis were the Core Support Barrel (CSB) upper and lower flanges. No further analysis was performed for these components since the original,[13], analysis had shown these areas to meet the requirements of Section 3.7.1 and the margin shown in Table 10 is conservatively based on the previous design loads. All other areas of the reactor internals for the Generic plant representing St Lucie 1 were reanalyzed using the asymmetric loads to compute stress intensities.

3.7.3 Stress Analysis of Reactor Internals

The core support structure components are analyzed for the loads resulting from a LOCA, both inlet or outlet break, in combination with the mechanical loads associated with normal operating conditions. The calculated stresses are combined to determine the maximum stress intensity which is compared with the membrane allowable of $2.4S_m$ or the membrane plus bending allowable of $3.6S_m$ (as applicable) as defined in the ASME Boiler and Pressure Vessel Code, Section III, Appendix F. The elastic material properties and stress allowables are conservatively taken at the reactor internals design temperature of 650°F.

The vertical loads, from the CESHOCK code, derived for the generic plant were conservatively used for the St Lucie plant specific stress analysis. The stresses from the vertical loads were combined with the stresses from the horizontal shears and moments to obtain the stress intensity for the reactor internals. The horizontal shears and moments were calculated for the generic plant representing St Lucie 1 by performing the dynamic structural analysis using the CESHOCK code.

For the generic plant (St Lucie 1), additional dynamic analyses were performed to compute the horizontal core support structure member loads using different values of friction resulting in different values of constraint at the CSB flange to reactor vessel ledge interface. The horizontal loads used in the analysis were conservatively based on the lower friction values, since the lower support beams and cylinder and the Control Element Assembly (CEA) shrouds. These components showed negligible increase in load with the lower friction value.

For an inlet break, the analysis of the CSB cylinder was based on the vertical and horizontal CESHOCK loads plus the stresses calculated for the shell effects from the ASHSD. For an outlet break, the stresses from the vertical and horizontal loads were combined with the buckling stresses from the SAMMSOR/DYNASOR results. The stresses on the reactor internals were largest for the inlet break.

3.7.4 Results of Component Analysis

Table 10 indicates that, for the asymmetric LOCA loads, all the core support structures meet the acceptance criteria as stated in Section 3.7.1. Although the reported margins are small, less than 5% for some components, the analysis was conservatively based on the CESHOCK loads using the lower friction value at the CSB flange to reactor vessel ledge interface. Use of the nominal friction case would increase the margin for all components listed except the lower support columns and cylinder which, because of a slight increase in load, shows negligible change in margin with increased friction.

The internal structures, which do not provide direct restraint to the core, were evaluated and it has been shown that their deflection will not adversely effect the function of the core support structures, satisfying the acceptance criteria of Section 3.7.1.

Margins for hot leg breaks are in general larger. It is therefore concluded that the St Lucie 1 reactor internals can successfully withstand LOCA breaks.

3.8 Evaluation of Combustion Engineering Fuel

This section compares the calculated fuel assembly component loads and stresses to the corresponding criteria discussed in Section 2.4.5.

The loads and stresses resulting from the postulated inlet and outlet breaks have been compared. The inlet break results are governing in each case, and in fact no component is overstressed or overloaded by the outlet break. Therefore, the discussion is limited to the effects of the inlet break.

The inlet break produces fuel assembly movement in two directions. Maximum stress intensities for each component have been calculated by combining the maximum stress intensities from each of the two directions by the square root of the sum of the squares (SRSS) method. Maximum spacer grid loads are reported separately for the two directions since channel closure across one grid width is not affected by loading across the other width.

3.8.1 Generic Plant Results (St Lucie 1)

As described in Sections 2.4.2, 2.4.3 and 2.4.4, two fuel assembly analyses were performed. The first analysis (Base Case) related friction at the core barrel flange and reactor vessel ledge to nominal operating loads. The results of this approach were overly conservative. In order to remove some of the

conservatism, a second (Revised Model) analysis was performed, which accounted for an increased value of friction at the flange. The stresses and loads calculated from both analyses are presented in Appendix A, and discussed below.

The ratios between the maximum stresses and maximum loads for the two cases are also presented. Each ratio is equal to the revised model result divided by the base case result.

3.8.1.1 End Fitting Castings and Posts

Table A-2 in A lists the maximum end fitting stress values along with the allowable values.

The maximum predicted stress values are less than the stress criteria.

3.8.1.2 Upper End Fitting Holddown Springs

The standard Combustion Engineering reload design includes holddown springs which are designed to have shear stresses below the criterion value (99,000 psi) at solid height. Therefore, no specific calculation was performed as part of the asymmetric loads evaluation.

3.8.1.3 Guide Tubes

Table A-2 in Appendix A lists maximum stress intensities for the guide tubes. As discussed in Section 2.4.5.4, there is no criterion on guide tube stress for the large break LOCA event. Yield strength of the guide tube material is referenced for information, and guide tube stress values are discussed further in Section 3.8.3.

3.8.1.4 Fuel Rods

Maximum fuel rod stress values are listed in Table A-2 of Appendix A. The stress criterion is also provided.

The maximum predicted stresses are less than the criterion.

3.8.1.5 Spacer Grid Impact Loads

Spacer grid impact loads are determined directly in the CESHOCK detailed core model described in Section 2.4.4. The impact loads for the generic plant fuel are listed in Table A-3 of Appendix A. Also shown are the spacer grid impact strengths from Table A-1 corrected for operating temperature.

Two categories of grid impact loads are listed in Table A-3. The one-sided load type corresponds to the case where a freely-moving bundle impacts an adjacent assembly or the core shroud, or where a free-standing bundle is impacted by another assembly. Thru-grid loads correspond to cases in which an assembly already rests against the shroud or another assembly and is then impacted on its opposite face. These two load categories have been distinguished in both the analysis and test models.

Except for loads on peripheral fuel assemblies, the grid strength is greater than the loads imposed on the grids during the postulated LOCA event.

In the row of fuel assemblies chosen for dynamic analysis, a total of four spacer grids are predicted to exceed the allowable load (two in each of the two peripheral assemblies). The maximum thru-grid loading is predicted for one of the same grids subject to a high one-sided loading.

Figures A-6 and A-7 show the core-wide distribution of one-sided and thru-grid loadings for all fuel assemblies in the row, for the case where the maximum loads were predicted.

The beneficial effect of irradiation on spacer grid strength is discussed in Section 3.8.2. Irradiation will increase grid strength by a factor of at least 1.5 by the time of fuel discharge, which is sufficient to provide the required load capability.

An evaluation of the effects of reduced channel flow area in peripheral spacer grids is presented in Appendix B. Fuel temperature calculations are presented to demonstrate core coolability following the grid loadings induced by the postulated pipe break at the vessel inlet nozzle.

3.8.2 Effects of Operating Conditions on Zircalloy Components

As discussed in the preceeding sections, maximum calculated guide tube stresses exceed the BOL unirradiated yield strength of the material, but do not violate any structural criteria. In addition, the maximum calculated spacer grid impact loads exceed the BOL unirradiated grid strengths, but are to be addressed by a coolability analysis (Appendix B).

For information, this section presents a discussion of the effects of irradiation and high strain rates on zircalloy mechanical properties. Both conditions will make zircalloy components less prone to permanent deformation than

indicated by out-of-pile testing.

3.8.2.1 Guide Tubes

Figure A-9 of Appendix A shows the effect of irradiation of the guide tube yield strength at operating temperatures. These data were obtained at the standard ASTM tensile test strain rate (0.00008 in/in/sec.). Figure A-10 depicts the estimated yield strength function at a strain rate which is representative of that occurring during the LOCA transient (0.1 in/in/sec.).

The axial distribution of maximum guide tube stresses from the generic plant analysis is shown in Figure A-11. By comparing these stresses to Figure A-10, it can be seen that the effects of strain rate and irradiation will begin to limit the region of permanent distortion after only a short period of reactor operation.* It should also be pointed out that the maximum stresses shown in Figure A-11 do not occur over all five guide tubes, nor over the full length of the span between grids. They are in fact confined to one side of two guide tubes, at a location near the spacer grids. The other stresses in the section of the fuel assembly would be considerably lower.

The ability of the guide tube material to withstand a given strain without fracture (at exposures lower than those estimated to be necessary to achieve a certain yield strength) is provided in Figures A-13 and A-14. Figure A-13 shows the total elongation (plastic) capability of the material as a function of irradiation, and Figure A-14 shows the total strain (elastic plus plastic) capability.

The guide tube stress calculation was performed under the assumption of elastic behavior, so only elastic strains can be obtained from the analysis. These are shown on Figure A-15 as a function of axial position. It can be seen by comparison with Figure A-14 that the maximum calculated elastic strain is lower than the material total strain capability. (The actual guide tube strains would be somewhat different in an elastic-plastic analysis; however, these differences should be small since each fuel assembly is still deflection-limited by the close proximity of surrounding assemblies and the reactor internals.) Therefore, the calculated elastic guide tube stresses should not produce fracture of the St. Lucie 1 plant guide tubes.

3.8.2.2 Spacer Grids

The effect of strain rate on spacer grid strength has already been accounted for in the dynamic test simulation method discussed in Section 2.4.2.

---

* The relationship between fluence and irradiation is approximately three weeks at full power per 10^{20} nvt.

The Combustion Engineering spacer grid design has been shown by testing to exhibit a yielding characteristic rather than buckling behavior, so that the grid strength at a given fluence equals the ratio of the yield strength at that fluence divided by the unirradiated yield strength (both at high strain rates).

The effect of irradiation at an extremely high strain rate (4.0 in/in/sec.) is shown in Figure A-16. The local strain rates in the spacer grid are unknown, but are believed to be at least this large.

This graph demonstrates that the spacer grids are expected to become at least 50% stronger by the time of discharge (about 6×10^{21} nvt.). Applying a factor of 1.5 to the spacer grid impact strengths would result in strength values higher than the maximum predicted impact loads in Table A-3 for the generic plant representing St. Lucie 1.

3.8.3 Summary of Fuel Evaluation

Calculations have demonstrated acceptable performance for all end fittings, holddown springs, and fuel rods in the generic plant representing St. Lucie 1. A limited number of spacer grids in the plant have calculated impact loads in excess of the BOL grid strength in a few peripheral core locations for the inlet break condition. The number of locations at which this condition exists is reduced as a function of time if credit is taken for spacer grid irradiated mechanical properties.

The vessel motions and internal asymmetric loads employed in the generic plant vessel internals and fuel evaluation result from analyses which assume a full unrestrained break at the inlet nozzle. In the St. Lucie 1 plant, the size of this break is in fact limited by restraining devices.

Although no direct scaling between results obtained for full area breaks and partial area breaks is possible, the impact loads are known to be a strong function of the vessel motion amplitudes. Since for partial area breaks, the internal hydraulic loads (fixed vessel) are less, and the vessel motions are approximately the same, it can be concluded that the impact loads will be the same or less. In the particular instance of the 4.0 square foot vessel inlet break, the internal hydraulic loads are approximately 60 percent of those resulting from a full area break, and the vessel motions are roughly the same as those resulting from a full break. It is suspected that the grid impact loads would be somewhat lower. For the 7.78 square foot break, they would be also about the same. Although no definitive conclusion can be drawn for the St. Lucie limited breaks, as the potential decrease in impact load may still be insufficient to pre-ent crushing of some grids, it is expected that crushing for St. Lucie 1 will be somewhat less than for the generic plant. In any case, the evaluation of core coolability for damaged peripheral grids is described in Appendix B.

4.0 CONCLUSION

The results of the analyses summarized in the preceding sections demonstrate that the existing design has significant capability to accommodate the postulated events. Additional information [10,11] which has become available since the August 1977 report, and which reinforces our contention, stated in that report, demonstrates that such events are of an acceptably low probability and cannot happen in the manner postulated for this analysis. The foregoing reaffirms our conclusion that the design of St Lucie Unit 1 is acceptable.

5.0 REFERENCES

1/ "PLAST - An Elasto-Plastic Computer Program for Stress Analysis of 3-D Piping Systems and Components Subject to Dynamic Forces", submitted to the NRC as ETR-1001 - Ebasco Topical Report.

2/ St. Lucie Unit No. 1 FSAR, Docket No. 50-335, Amendment 44.

3/ "RELAP 4 - A Computer Program for Transient Thermal Hydraulic Analysis of Nuclear Reactors and Related Systems", User's Manual, ANCR-NUREG-1335.

4/ Fabic, S., "Computer Program WHAM for Calculating Pressure, Velocity and Force Transients in Liquid Filled Piping Network", Kaiser Engineering Report No. 67-49-R, November 1967.

5/ "ICES STRUDL II - The Structural Design Language Engineers User's Manual", MIT Press, Cambridge, Massachusetts, 1968.

6/ "ADMASS - A Computer Code for Fluid Structure Interaction Using the Finite Element Technique", Ebasco Services, Incorporated, 1979.

7/ "DAGS-CENPD 168, Revision 1 - Design Basis Pipe Breaks", September 1976.

8/ "DFORCE - Design Basis Pipe Breaks", September 1976.

9/ "MSC/NASTRAN - User's Manual", McNeal Schwandler Corporation, Los Angeles, California (1978).

10/ "WCAP 9570 Class 3 - Mechanistic Fracture Evaluation of Reactor Coolant Pipe Containing a Postulated Circumferential Thru Wall Crack", S. S. Palusamy and A. J. Hartmann, October 1979.

11/ Ayers, D. J. and T. J. Griesbach, "Opening and Extension of Circumferential Cracks in a Pipe Subjected to Dynamic Loads", Fifth International Conference of Structural Mechanics in Reactor Technology, Berlin, Germany, 1979.

12/ Griffin, J. H., "MEC-21 - A Piping Flexibility Analysis Program", TID-4500 (31st edition), LA-2924, UC-38, July 14, 1964.

13/ "Topical Report on Dynamic Analysis of Reactor Vessel Internals Under Loss of Coolant Accident Conditions with Application of Analysis to CE 800 MWe Class Reactors", CENPD-42, 1971.

14/ "CESHOCK - A Computer Code to Solve the Dynamic Response of Lumped Mass System", Described and Verified in above Reference 13.

15/ "ASHSD - A Dynamic Stress Analysis Code of Axisymmetric Structures Under Arbitrary Loading", Described and Verified in above Reference 13.

16/ "SAMMSOR - A Finite Element Program to Determine the Stiffness and Mass Matrices of Shells of Revolution", Described and Verified in above Reference 13.

17/ "DYNASOR - A Finite Element Program for Dynamic Non-Linear Analysis of Shells of Revolution", Described and Verified in above Reference 13.

18/ Gerber, T. L., "Plastic Deformation of Piping Due to Pipe Whip Loading", ASME Paper 74-NE-1, 1974.

19/ Combustion Engineering Inc., "Method for the Analysis of Blowdown Induced Forces in a Reactor Vessel", CENPD-252-P, Dec. 1977 (Proprietary).

20/ "ANSYS" Swanson Analyses Systems, G.J. DeSalvo, J.A. Swanson, 1975.

6.0 TABLES AND FIGURES

TABLE 1
ST. LUCIE 1

NORMAL AND SEISMIC SUPPORT LOADS (X10^6 LB.)

CONDITION LOAD	NORMAL OPERATING		OBE SEISMIC			DBE SEISMIC		
	DEAD WEIGHT	THERMAL + DEAD WEIGHT	±X	±Y	±Z	±X	±Y	±Z
H1	0	.028	.005	.002	−.644	.011	.005	−1.288
V1	.666	1.155	.032	.336	−.046	.064	.070	−.092
μV1	±.195	±.350						
H2	0	−.091	1.220	.001	+.355	2.452	.003	+.710
					−.264			−.528
V2	.664	.720	.017	.253	.300	.035	.507	.761
μV2	±.195	±.215						
H3	0	.079	1.139	−.019	.270	2.278	−.038	.540
				−.060	−.349		−.120	.698
V3	.634	.741	.367	.023	.743	−.006	.506	.746
μV3	±.195	±.215						
Z11	0	0	0	0	±.195	0	0	±.390
Z12	0	0	0	0	±.197	0	0	±.394
Y1	.300	0	.016	−.019	0	.033	−.039	0
Y2	.300	.315	−.057	.155	.060	−.114	.311	.121
Y3	.300	1.009	.080	.417	−.071	.173	.035	.143
Y4	.300	.320	−.054	.152	.058	−.108	.305	.116
X	0	0	0	0	0	0	0	0
μY	±.375	±.300						

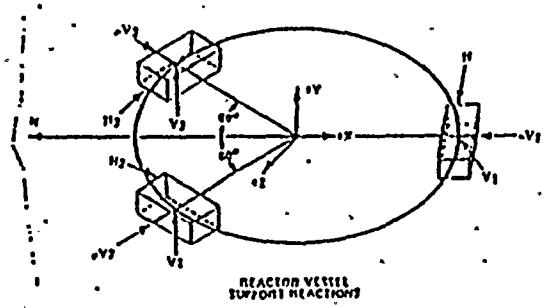

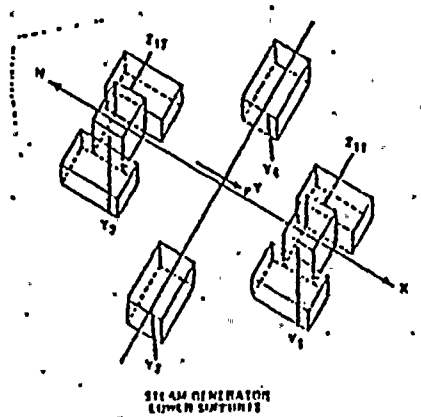

Table 2

Comparison of Peak Calculated and Design Seismic (DBE) Loads at Representative Locations

	Design (Kips)		Calculated (Kips)	
	Horizontal	Vertical	Horizontal	Vertical
Cold Leg Spt	2,455	1,268	522.6	354.6
Hot Leg Spt	1,293	762	515.0	429.4

Table 3

St. Lucie Unit #1

RV SUPPORT MAX ABS REACTIONS (KIPS) - LOCA + SEISMIC (SRSS)*

4 FT^2 CLG BREAK AT NOZZLE 1A OR 2A+

LOCATIONS	RV SPPT STIFFNESS VALUES	
	K_H = 64.62 x 10^6 lb/in	K_H = 77.54 x 10^6 lb/in
	K_V = 59.71 x 10^6 lb/in	K_V = 75.83 x 10^6 lb/in
#1A SPPT		
Vertical	1397	2317
Horizontal	1502	1587
#1B SPPT		
Vertical	2800	2251
Horizontal	5331	5473
Hot Leg SPPT		
Vertical	3458	3048
Horizontal	7493	7777

* For LOCA + Nop reactions, add these values to the vertical results:

#1A	SPPT	710. K
#1B	SPPT	726. K
Hot Leg	SPPT	1157 K

+ For break at nozzle 1B or 2B, the loads on the cold leg supports would be reversed

Table 4

St. Lucie 1 Reactor Pressure

Vessel Support Capacity

Steel support structure	-	horizontal	8400 kips* (concrete is limiting)
Steel support structure	-	vertical downward	12000 kips
Reactor Cavity Wall	-	horizontal	~13000 kips**
Reactor Cavity Wall	-	vertical	not limiting
Reactor Support Pads	-	horizontal	See Figure 4
Reactor Support Pads	-	vertical	See Figure 4

* Load on individual girder

** Allowable resultant asymmetric mechanical load transmitted along girders to concrete, based on rebar mean axial stress being within yield.

TABLE 5

STEAM GENERATOR LOWER SUPPORT CALCULATED AND DESIGN LOADS

(REFER TO TABLE 1 FOR SYMBOLS) SUPPORT	CL GUILL NO. 1 + OBE (RSS)	HL GUILL NO. 2 + OBE (RSS)	DESIGN LOAD LOCA + OBE
Z11	727	42	3,600
Z12	806	40	−1,868*
FRONT Y1	−406.9	−2487.7	−1,770
SIDE Y2	−756.5	−1176.4	−1,737
BACK Y3	−605.0	+1249.0	− ,691
SIDE Y4	−300.1	−1175.9	−1,734
X-STOP		−5194.9	5,643
S	78	278	− ,301
Z1	194	40	−1,574
Z2	301	40	1,300

(K AND FT − KIPS)

℄ C STEAM GENERATOR/ SLIDING BASE SUPPORT SKIRT INTERFACE	(H L GUILL) LOCA	RSS LOCA & OBE	SLIDING BASE DESIGN LOADS
Fx	5205	5205	5653
Fy	−3582	− 3582	−2,471.0
Fz	−	6.8	11.0
Mx	8	418.3	32.0
My	65	33.6	24.0
Mz	−4609	4614	− 1003

*A NEGATIVE SIGN MEANS TENSION

Table 6

St. Lucie Unit #1 Reactor Coolant System Reactor Pressure Vessel and Reactor Coolant Pump Nozzle Loads Due to a 4 ft^2 Reactor Vessel 1A Inlet Nozzle Guillotine Break

PIPE RUPTURE RSS MOMENT (In-Kips)

Nozzle	RCP Snubber Acting	RCP Snubber Not Acting	Seismic Moment (In-Kips)	Allowable Moment (In-Kips)
RCP Discharge	109,300	109,600	5,910	96,810
RCP Suction	50,500	54,550	7,256	78,965
RV Inlet	71,750	71,910	5,272	78,965
RV Outlet	50,150	50,170	2,535	279,340

Table 7

St. Lucie Unit No. 1

Connected Piping Stresses Calculated vs. Allowable
4.0 sq. ft. CLG Inlet Break

Design Point (Refer to Figure 5)	Calculated Stress (Equ. 10 ASME)	Allowable Stress
1	39,070	48,600
2	75,152*	48,600
3	75,030*	48,600
5*	41,835	48,600
6*	43,475	48,600
7	47,690	48,600
8	33,430	48,600
19	20,171	48,600

* Functionability and integrity are assured if Level B (upset conditions) limits of the ASME Boiler and Pressure Vessel Code, Section III, Division 1 are not exceeded. Functionability is important at points 5 and 6 where the valve is. At points 2 and 3, these limits are exceeded. However, Level D (faulted limits) are not exceeded at these two points. Level D limits are used to demonstrate that integrity is maintained. Equation (9) at those two points would yield 45,043 psi and 44,479 psi respectively with an allowable of 48,600 psi.

Table 8

Generic Plant

Lateral Model Node Locations

NODE	DESCRIPTION
1	Ground
2	RV @ snubber location
3	RV
4	RV
5	RV @ nozzle
6	RV
7	CSB lower flange
8	CSB @ snubber location
9	CSB
10	CSB
11	CSB
12	CSB
13	CSB
14	CSB
15	CSB @ nozzle
16	CSB
17	CSB upper flange (top surface)
18	LSS
19	Core support plate (center)
20	Core shroud
21	Core shroud
22	Core shroud
23	Core shroud
24	Core shroud
25	Core shroud
26	Core shroud
27	Core shroud
28	Core shroud
29	Fuel alighment plate (center)
34 + 9i	Fuel
35	Fuel
36	Fuel
37	Fuel
38	Fuel
39	Fuel
40	Fuel
41	Fuel
42 + 9i	Fuel
79 + 4i	CEA shrouds
80	CEA shrouds
81	CEA shrouds
82	CEA shrouds
83 + 4i	CEA shrouds
99	UGS support plate

Table 9
Generic Plant

Vertical Model Node Locations

NODE	NODE LOCATION DESCRIPTION
1	CSB @ upper surface of lower flange
2	CSB @ snubbers
3	CSB @ lower section thickness change
4	CSB
5	CSB
6	CSB
7	CSB
8	CSB
9	CSB
10	CSB
11	CSB
12	CSB
13	CSB @ top of upper flange
14	LSS @ top of grid beams
15	Core support plate center
16	Fuel assembly @ CEF plate
17	Guide tubes
18	Guide tubes
19	Guide tubes
20	Guide tubes
21	Guide tubes
22	Fuel assembly @ UEF plate
23	Center of fuel alignment plate
24	Fuel rods
25	Fuel rods
26	Fuel rods
27	Fuel rods
28	Fuel rods
29	Base of core shroud
30	Core shroud
31	Core shroud
32	Top of core shroud
33	CEA's
34	CEA's
35	CEA's
36	CEA's
37	CEA's
38	Top of UGS support plate
39	Reactor vessel ledge
40	Reactor vessel @ outlet nozzle
41	Reactor vessel
42	Reactor vessel supports
43	Reactor vessel @ top of core shroud
44	Reactor vessel
45	Core shroud node

CALCULATED REACTOR INTERNALS STRESS MARGIN
GENERIC PLANT
(ST. LUCIE 1)

TABLE 10

CORE SUPPORT COMPONENT	STRESS MARGIN* (PERCENT)
CORE SUPPORT BARREL	
UPPER FLANGE	39%
UPPER CLYINDER	52%
CENTER CYLINDER	32%
LOWER CYLINDER	36%
LOWER FLANGE	2%
LOWER SUPPORT STRUCTURE	
SUPPORT COLUMNS	48%
BEAMS & CYLINDER	22%
CORE SUPPORT PLATE	6%
UPPER GUIDE STRUCTURE	
UGS FLANGE	19%
GRID BEAMS	2%
CEA SHROUDS	1%

* STRESS MARGIN AS DEFINED IN SECTION 3.7.1

FIGURE 1
RELAP4 MODEL FOR ST. LUCIE
PRIMARY COOLANT SYSTEM

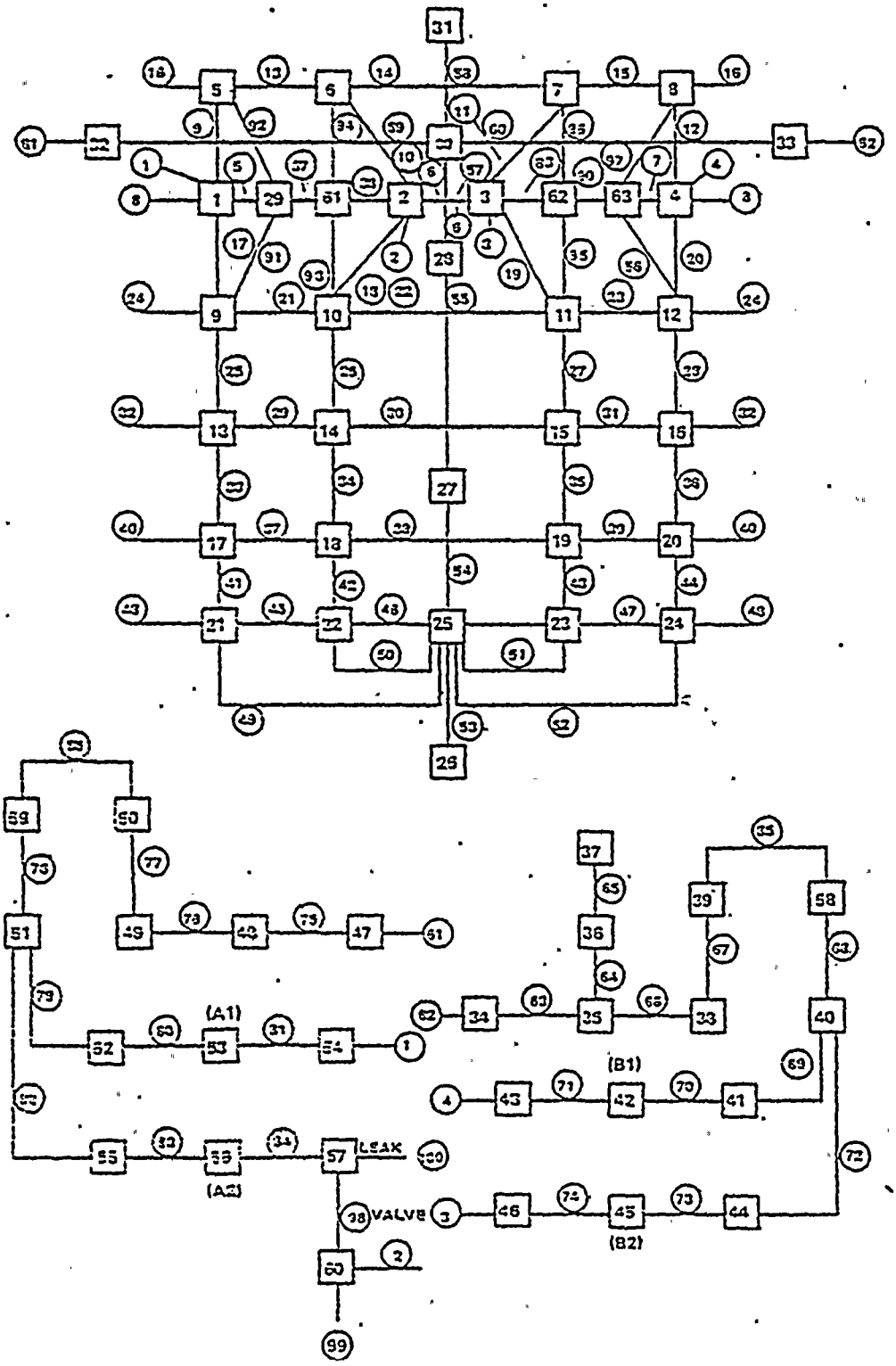

FIGURE 2
ST. LUCIE 1
RCS- WHAM/6 MODEL FOR IAL

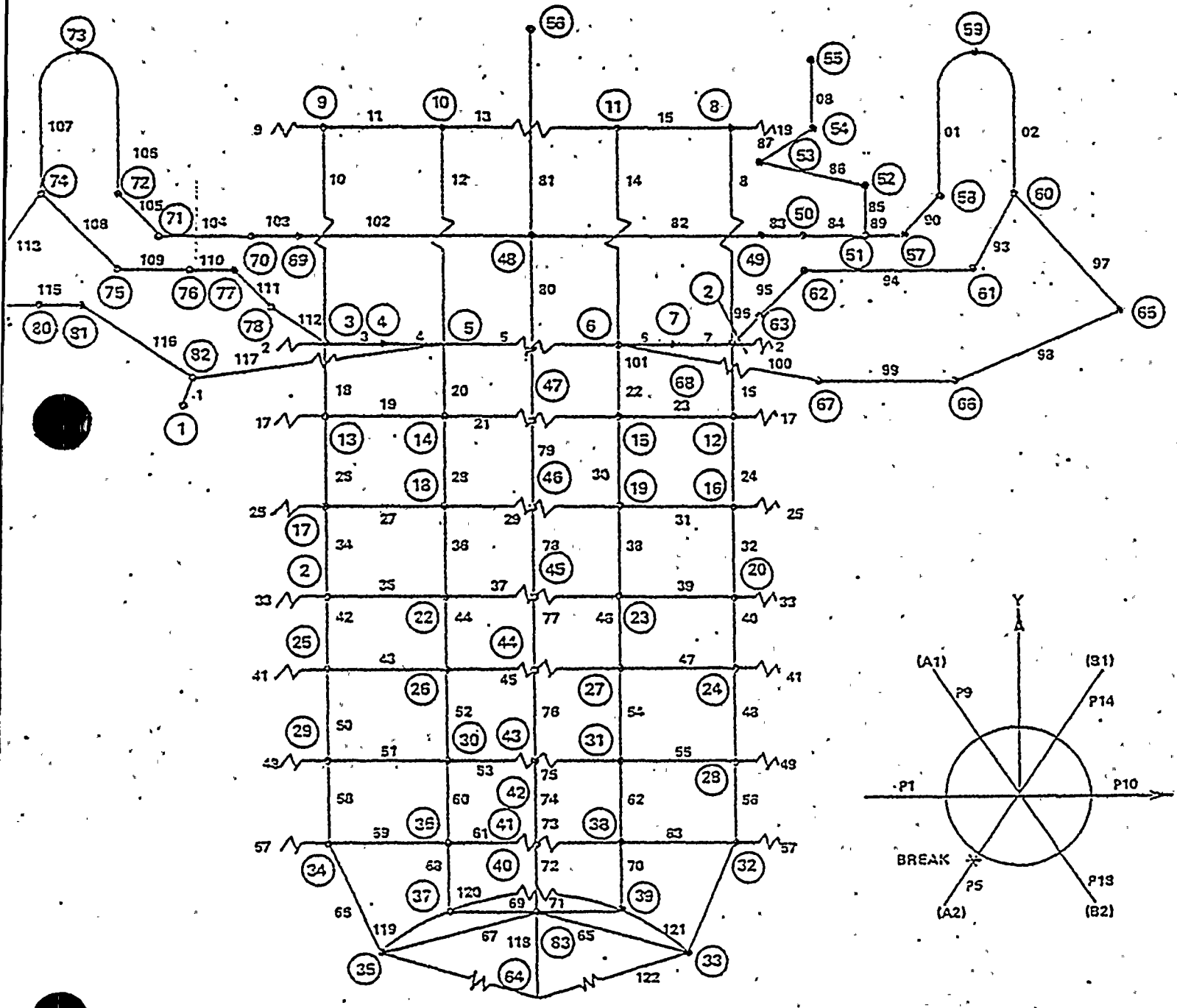

FIGURE 3A ST. LUCIE 1

REDUCED MODEL OF REACTOR INTERNALS

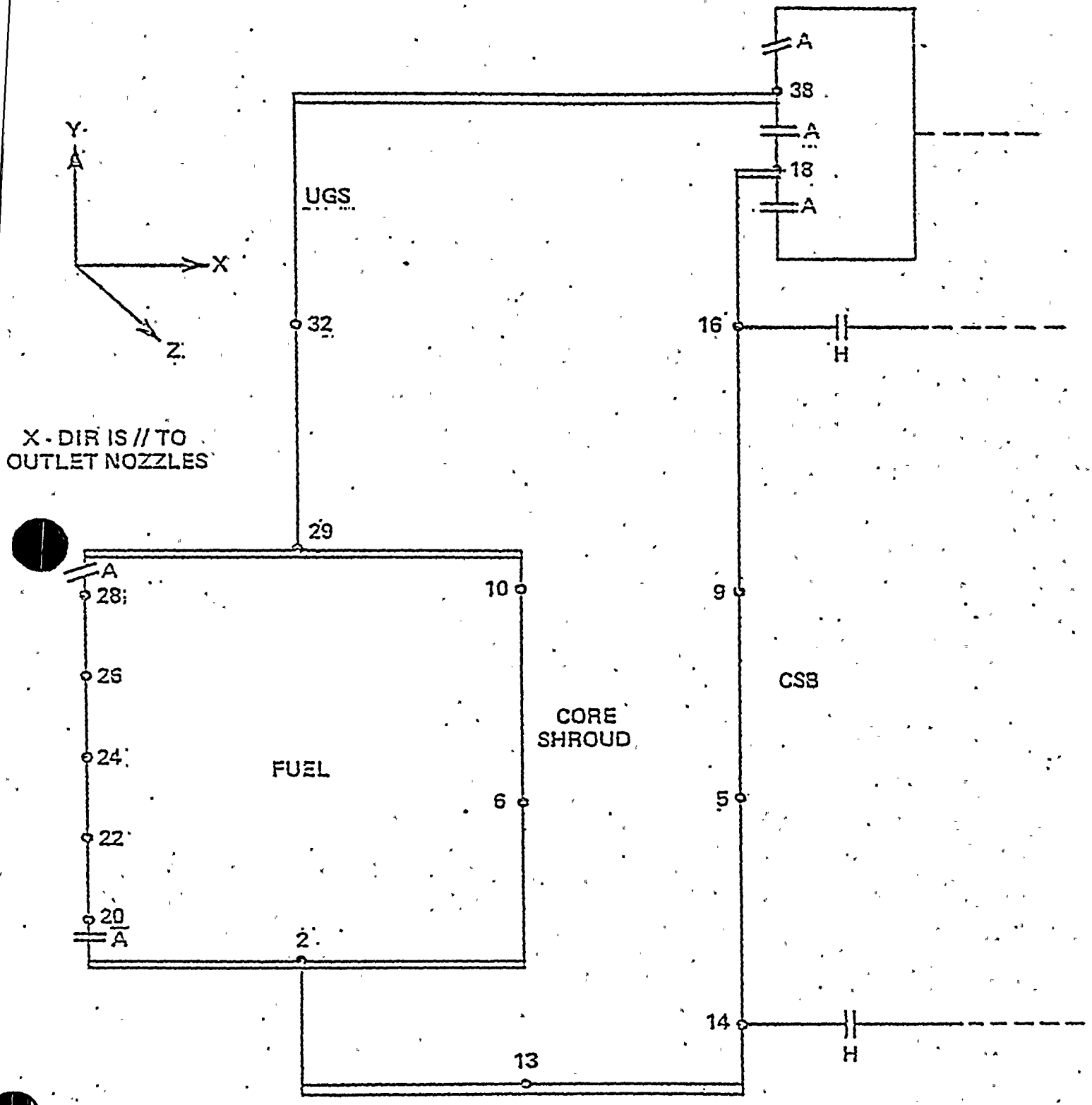

LEGEND

A = AXIAL GAP
H = HORIZONTAL GAP
// = PRELOADED COUPLING
= GAP COUPLING
= COLINEAR CONNECTOR

*SEE FIGURE 3b FOR DETAILS OF REACTOR VESSELS AND PIPING

FIGURE 3B ST. LUCIE 1

REDUCED MODEL OF REACTOR COOLANT SYSTEM

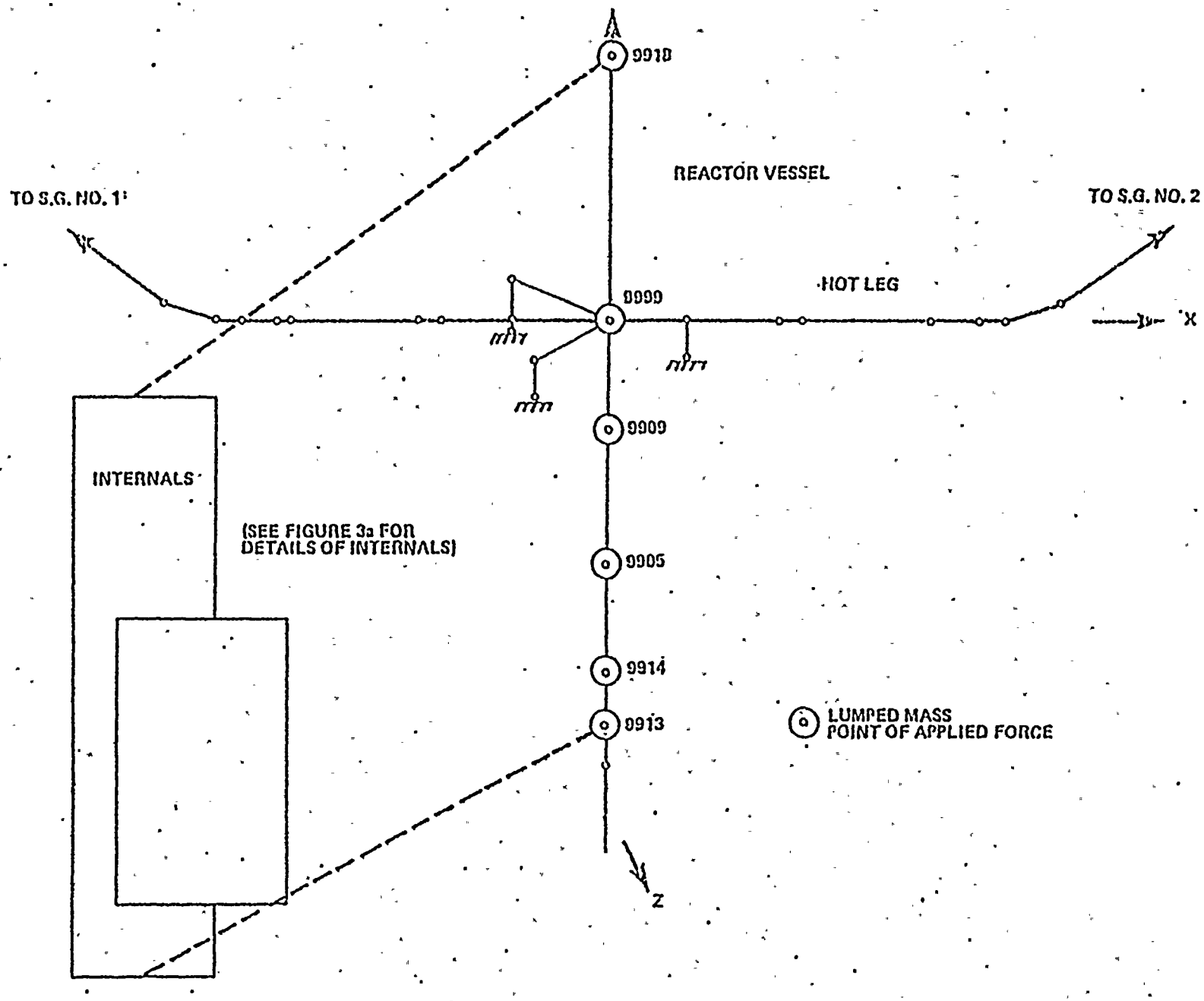

FIGURE 4 ST. LUCIE 1

REACTOR PRESSURE VESSEL SUPPORT PAD CAPABILITY

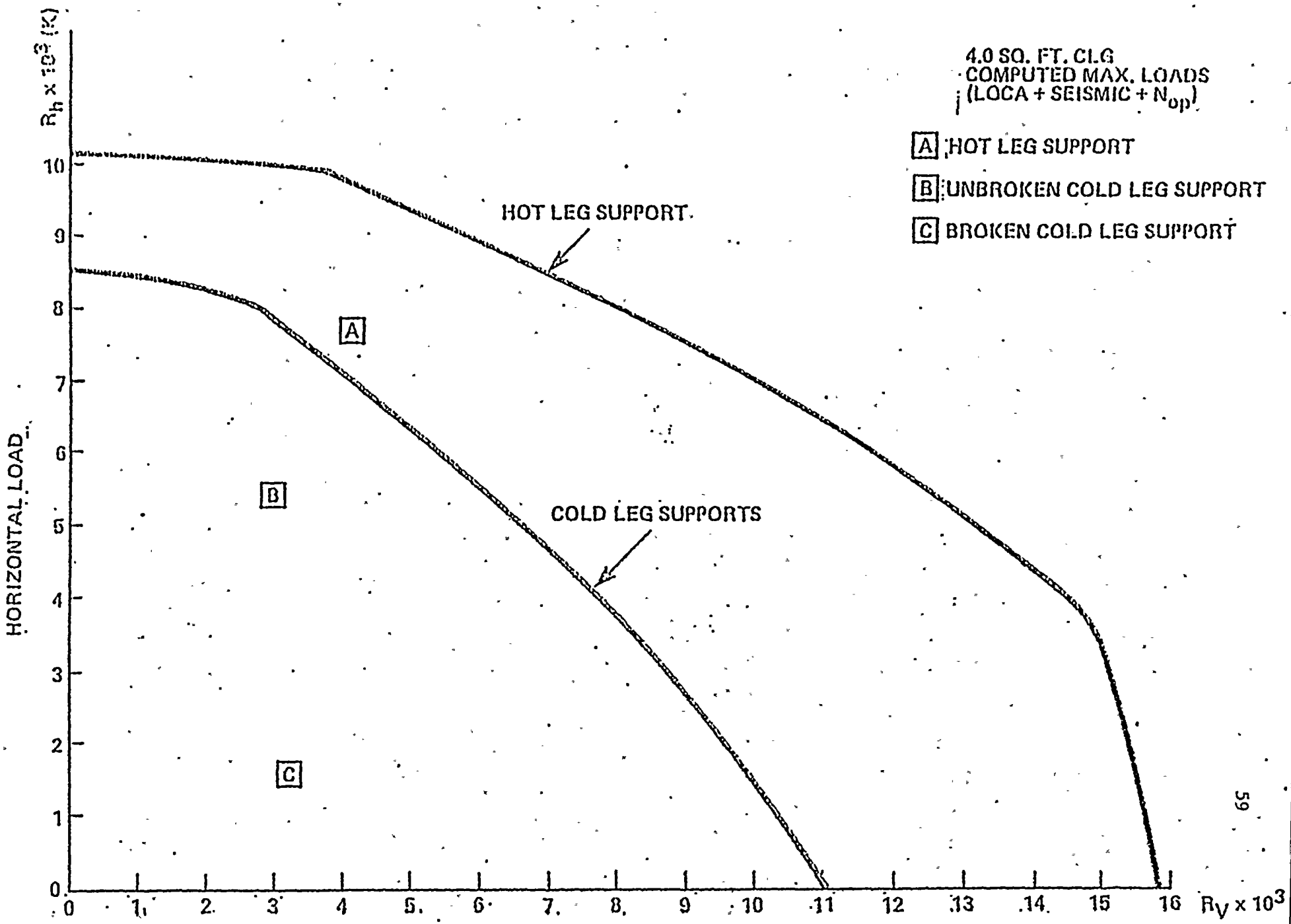

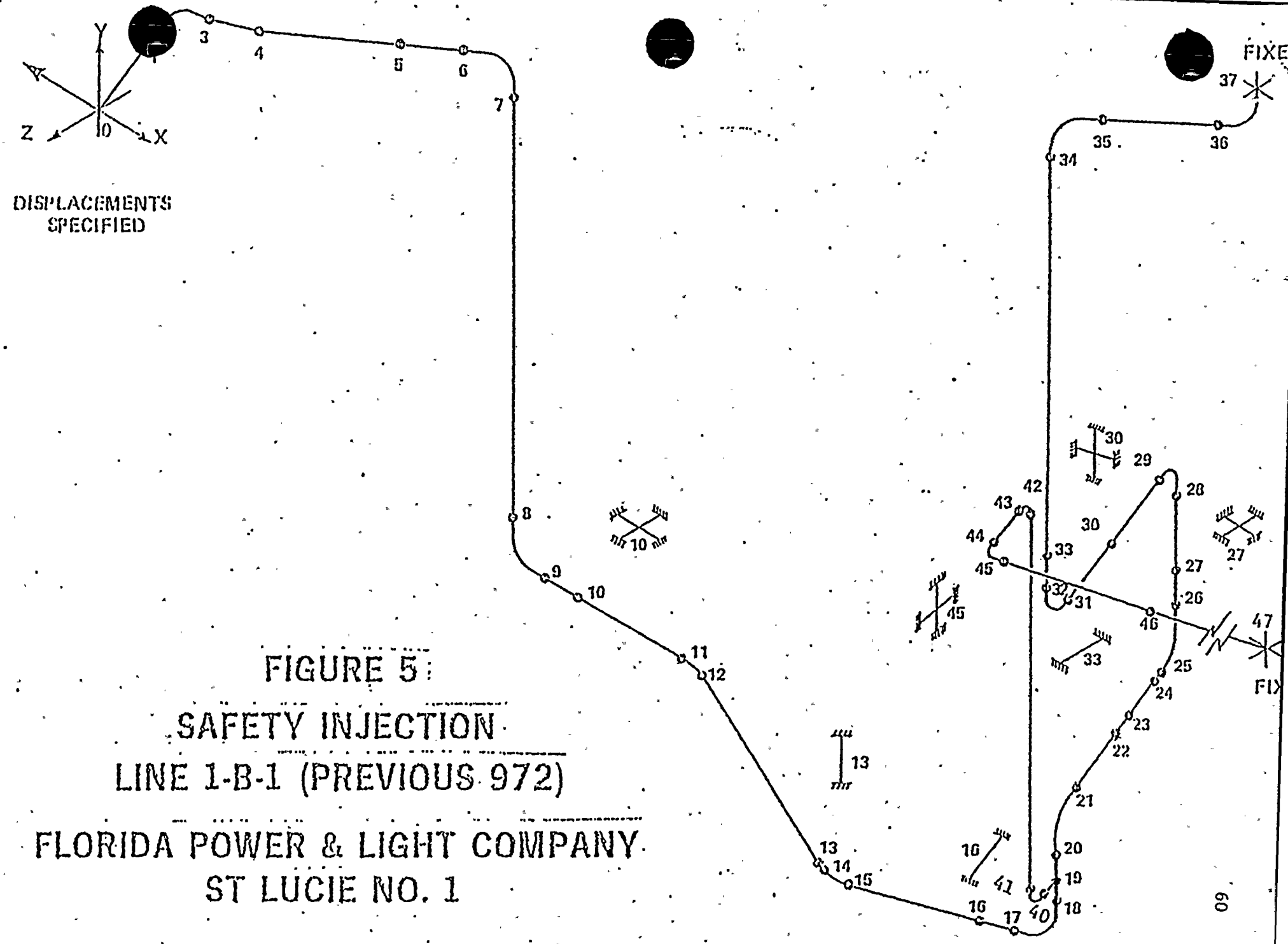

FIGURE 5:

SAFETY INJECTION

LINE 1-B-1 (PREVIOUS 972)

FLORIDA POWER & LIGHT COMPANY

ST LUCIE NO. 1

K+E 10 X 10 TO ½ INCH 7 X 10 INCHES KEUFFEL & ESSER CO. MADE IN U.S.A. 46 1323

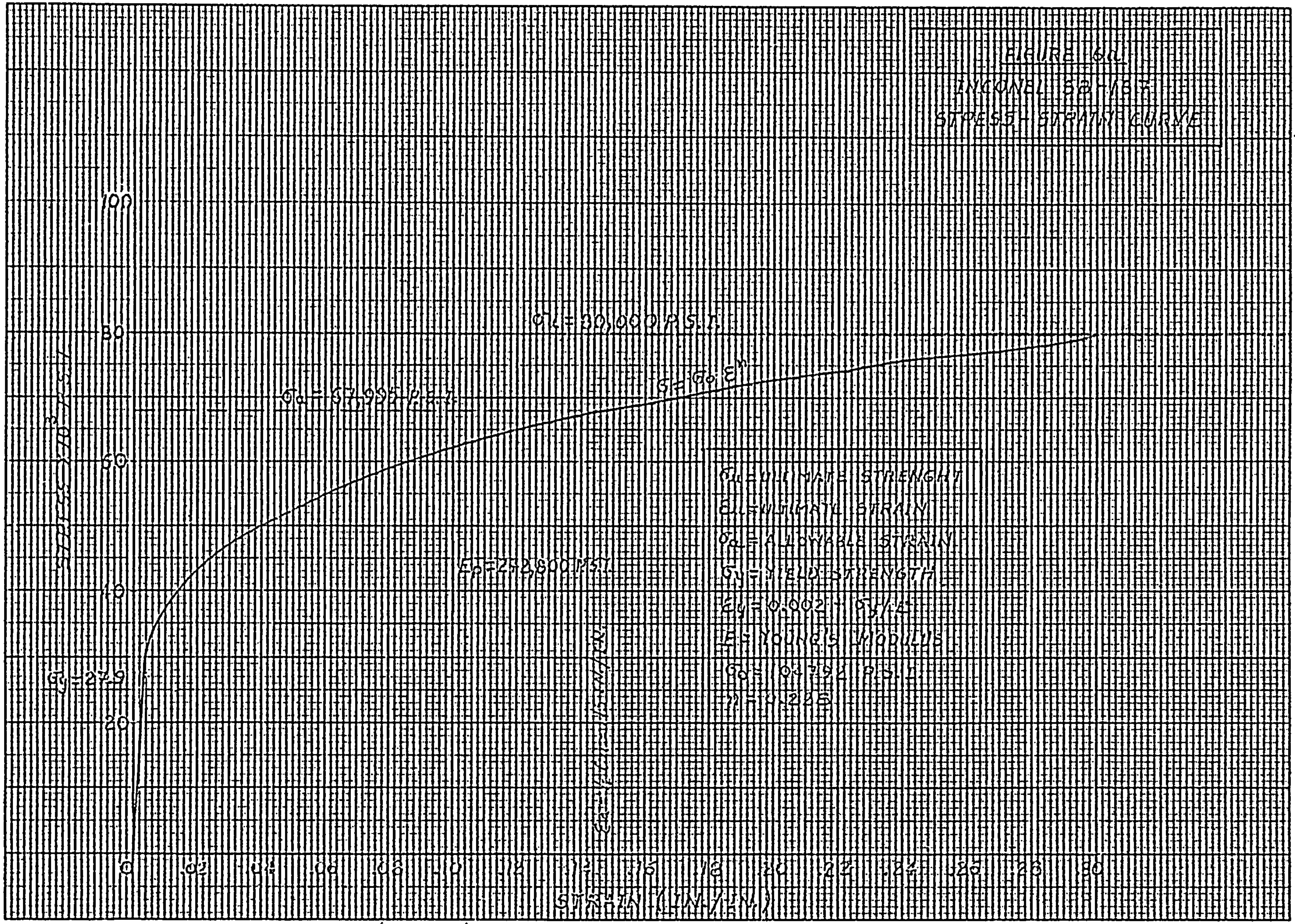

FIGURE 6b

C.E.D.M. MODEL
FOR
ST. LUCIE NO. 1

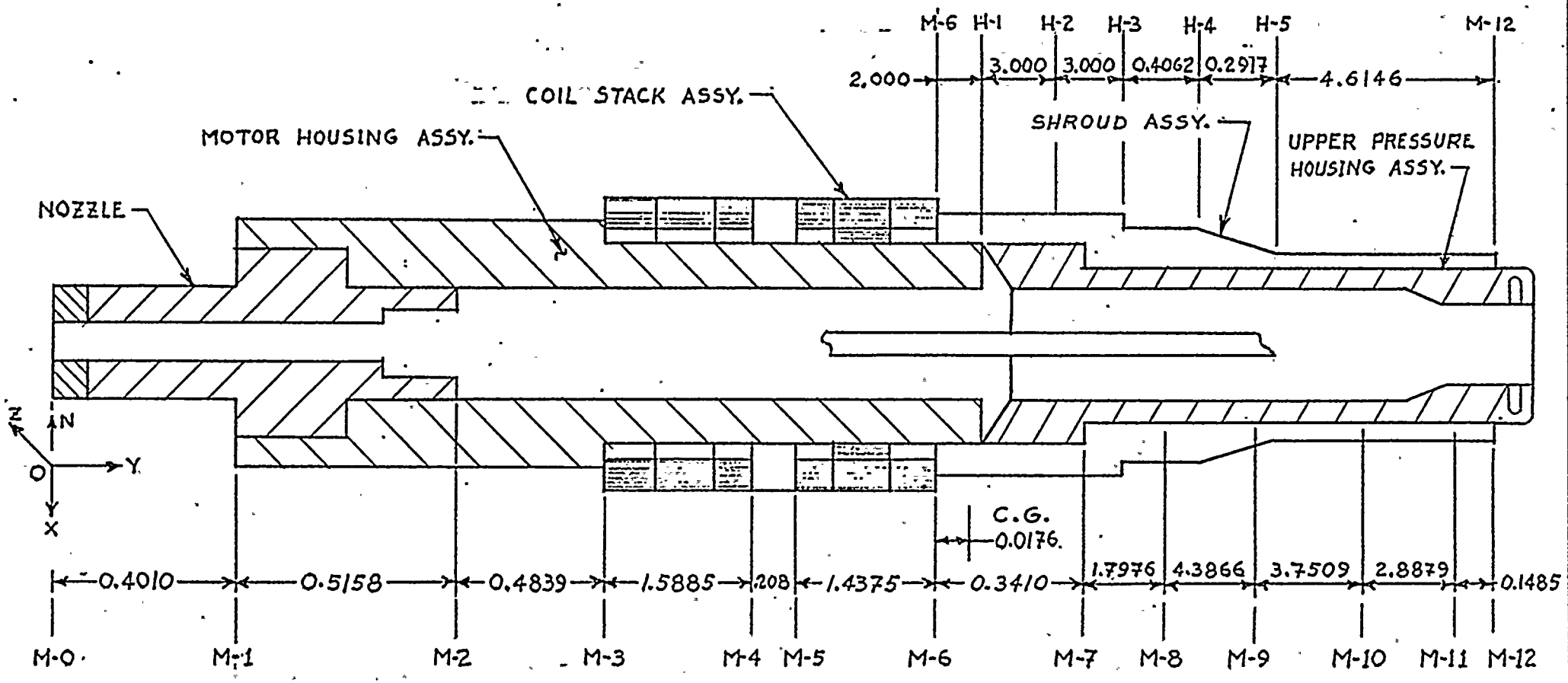

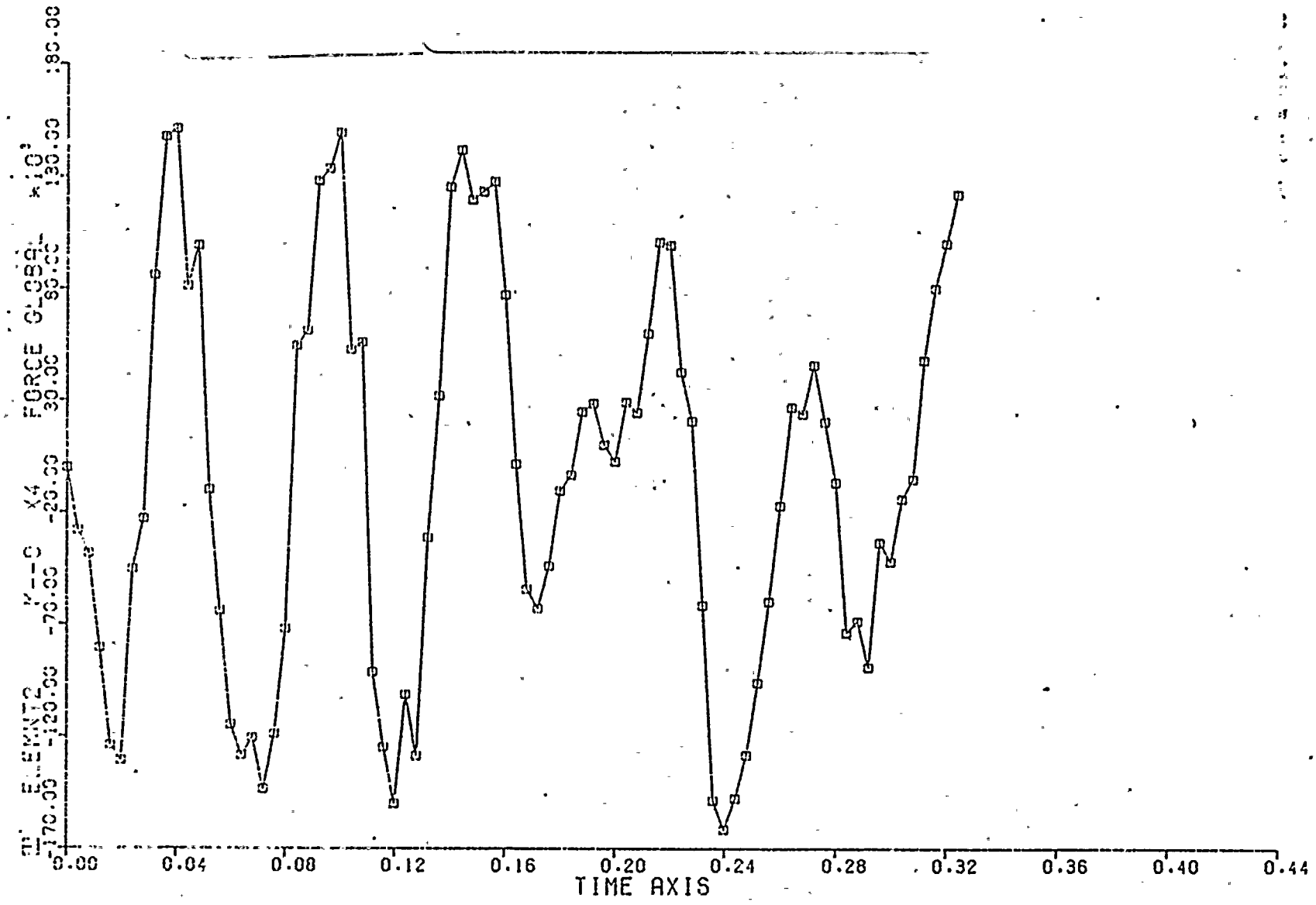

Figure 7a -Bending Moment at CEA Nozzle about x-axis

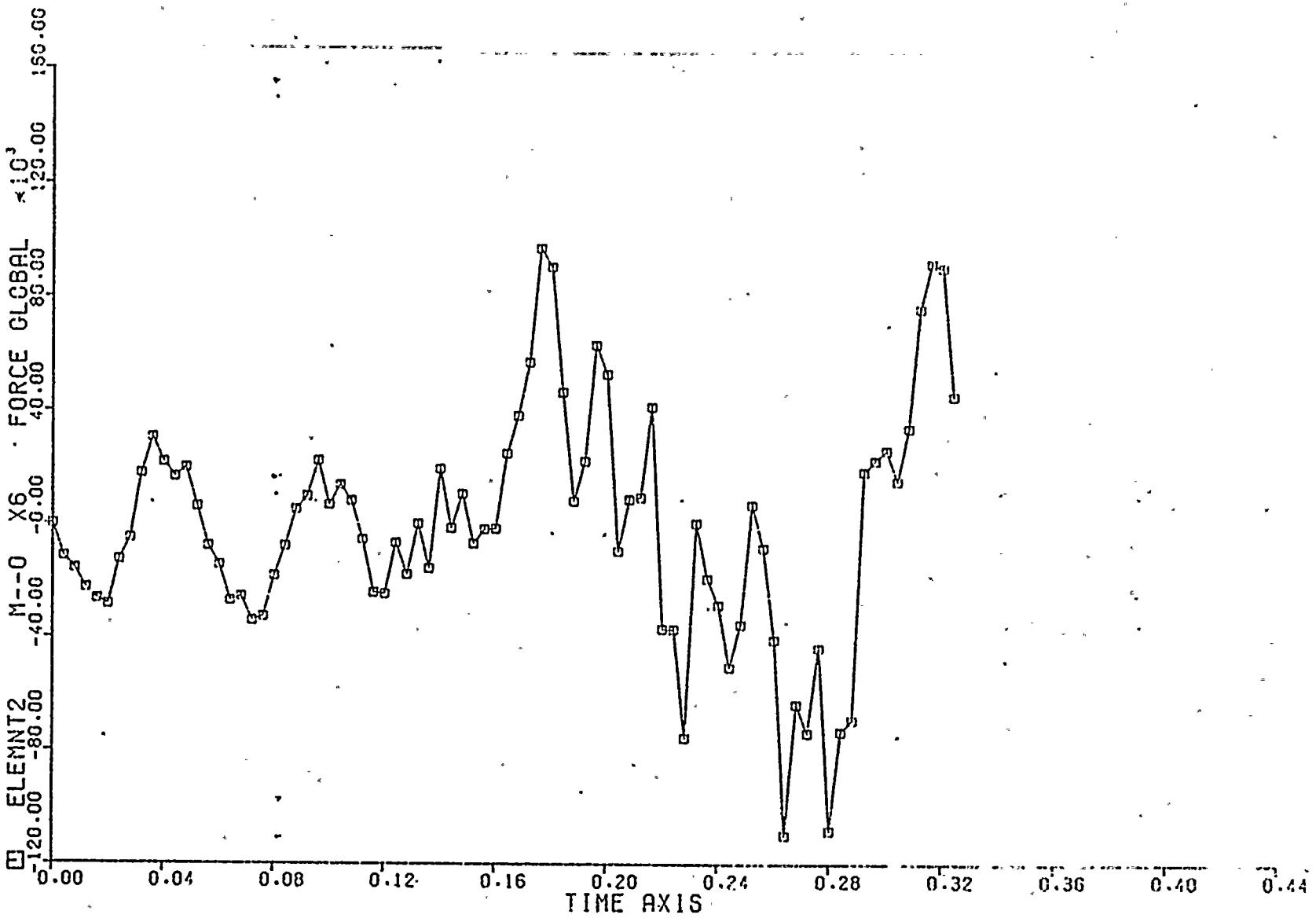

Figure 7b – Bending Moment at CEA Nozzle about x-axis

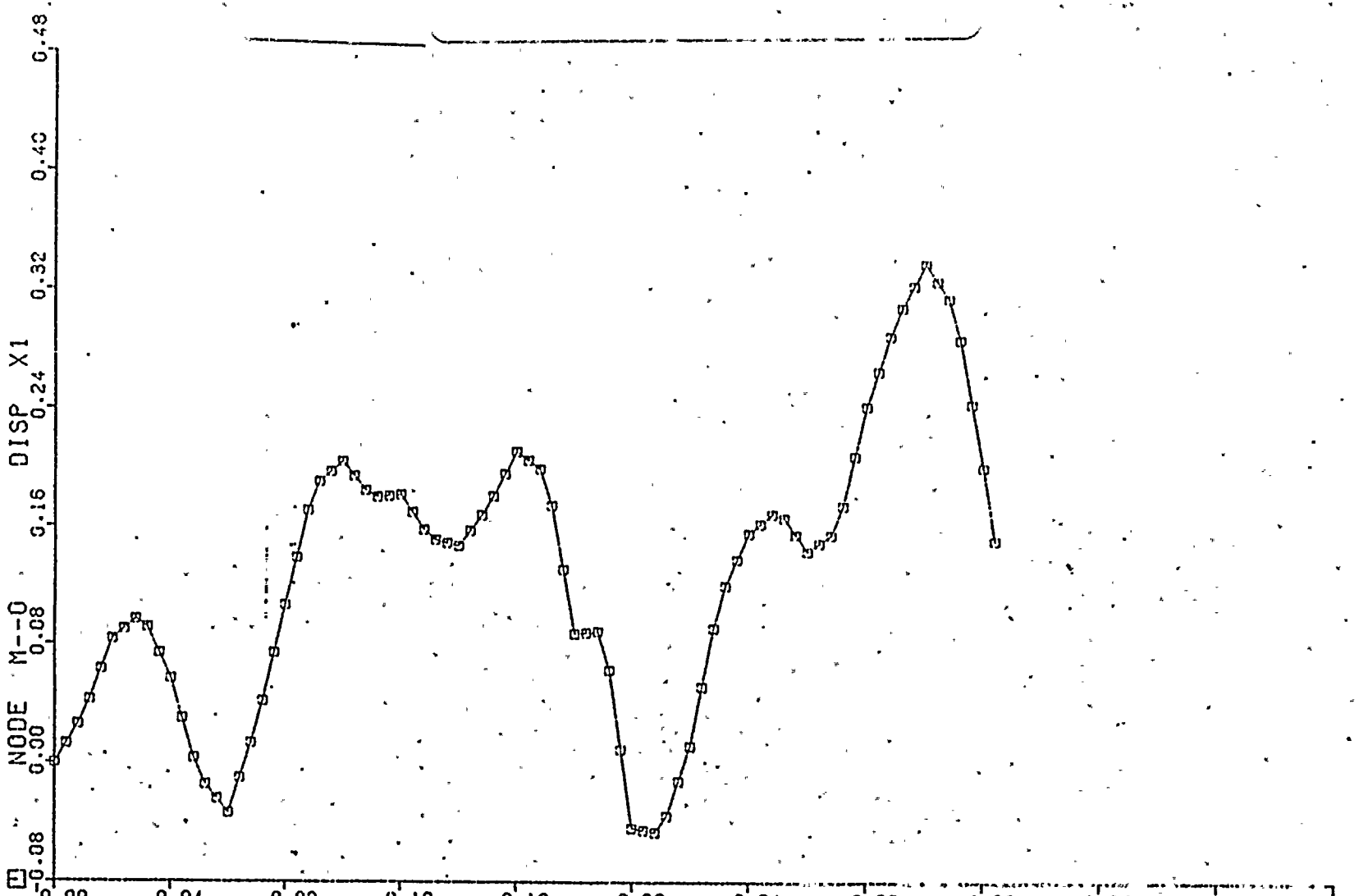

Figure 7c - CEDM Nozzle Displacement Time Histories -x Displacement

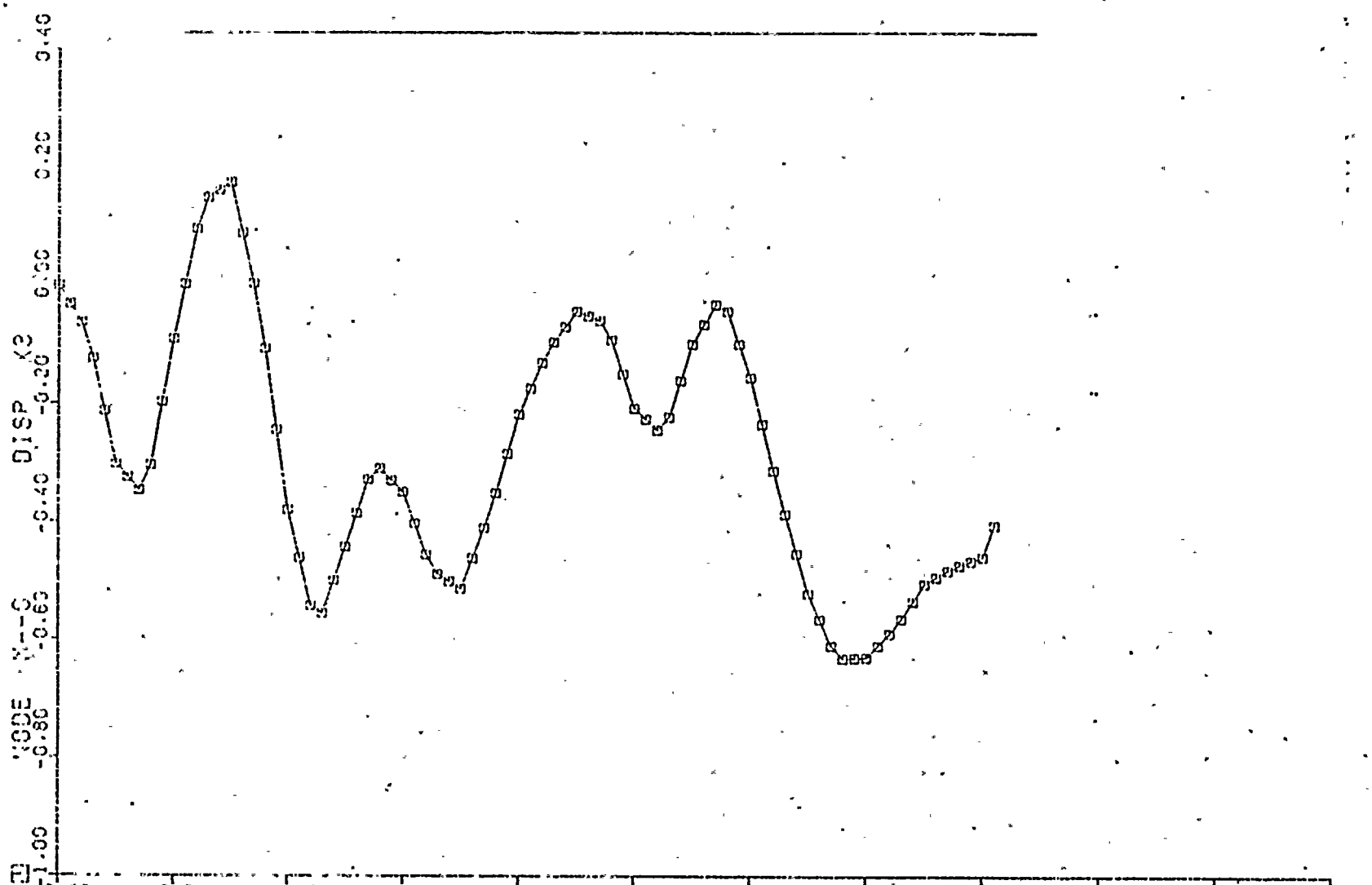

Figure 7d - CEDM Nozzle Displacement Time Histories - Y Displacements

FIGURE 23.

EVALUATION OF MOMENT IN C-DM NO. 11 INCONEL 5% Cr ST-TUBE JUNCTION NO. 1

ULTIMATE MOMENT (C-M) = 275,000 IN. LBS.

MAXIMUM ALLOWABLE MOMENT (0.5 M) = 149,900 IN. LBS.

PLASTIC FAILURE = 183,000 IN. LBS.

MOMENT X 10³ IN. LBS.

500
450
400
350
300
250
200
150
100
50
0

.08 .16 .24 .32 .40 .48

ROTATION

FIGURE 8

GENERIC PLANT

DETAILED LATERAL INTERNALS MODEL

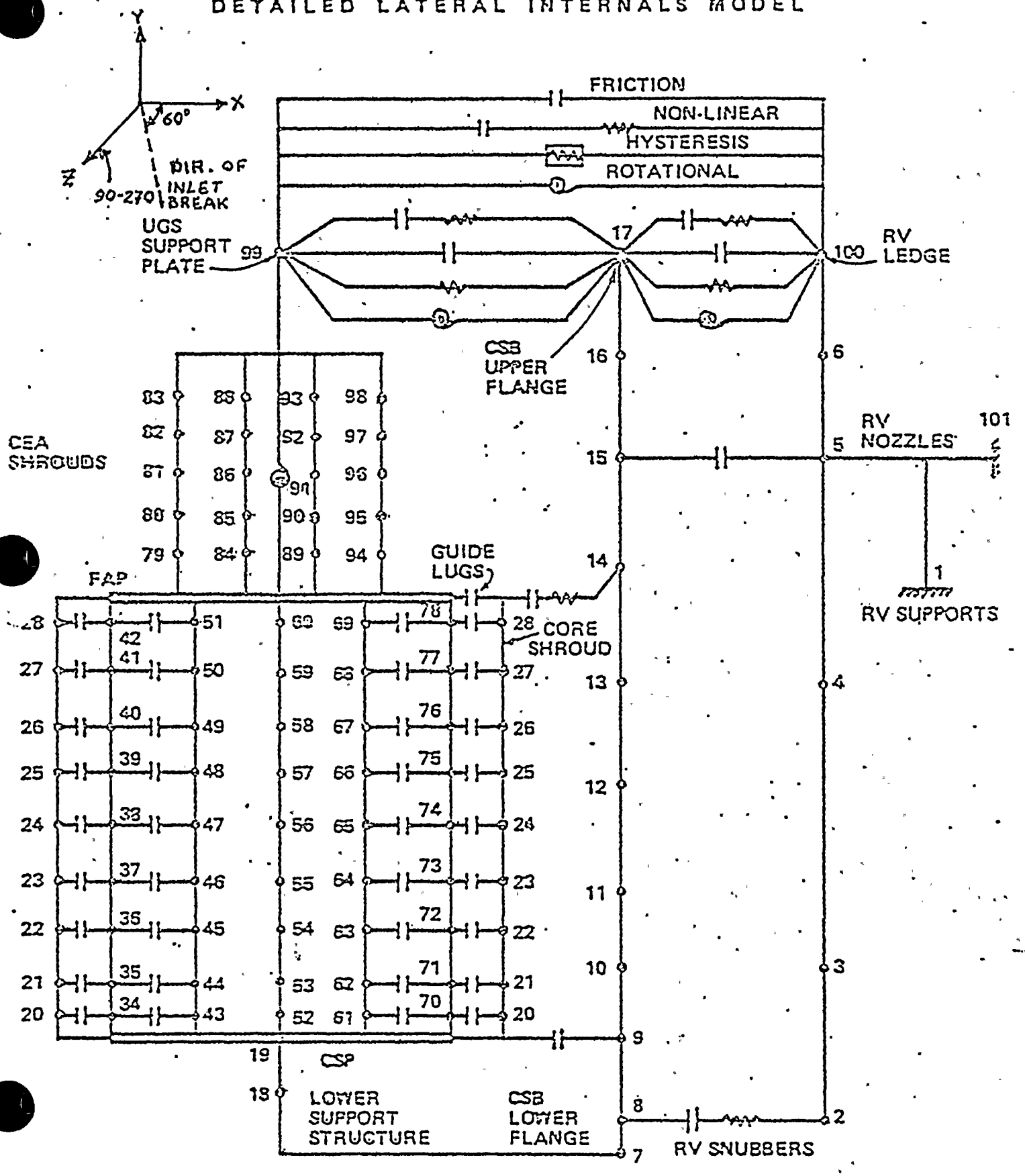

DETAILED VERTICAL MODEL

FIGURE 9

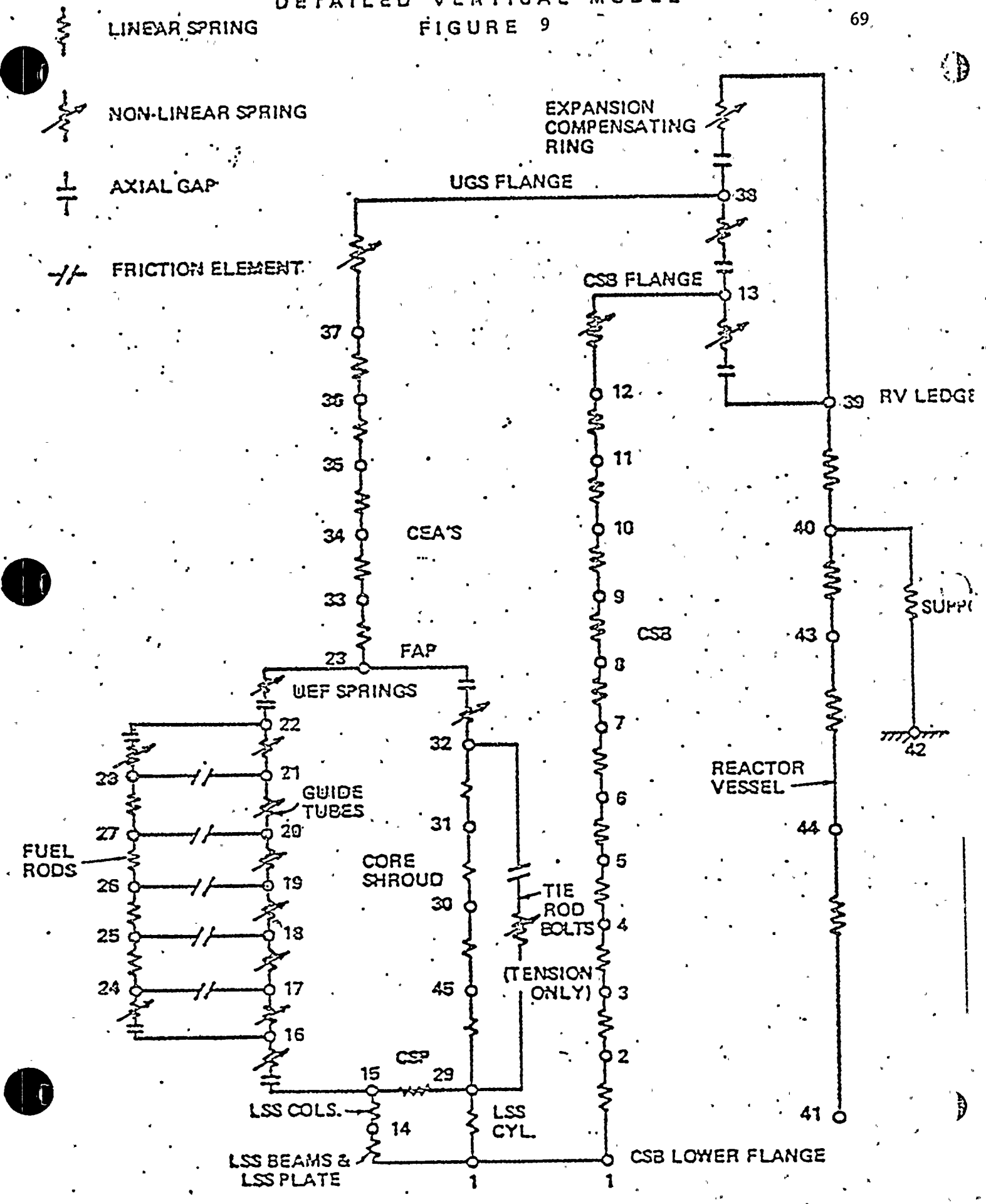

FIGURE 10.

GENERIC PLANT COLD LEG BREAK CORE SUPPORT BARREL TOTAL LOADS PARALLEL TO HOT LEGS

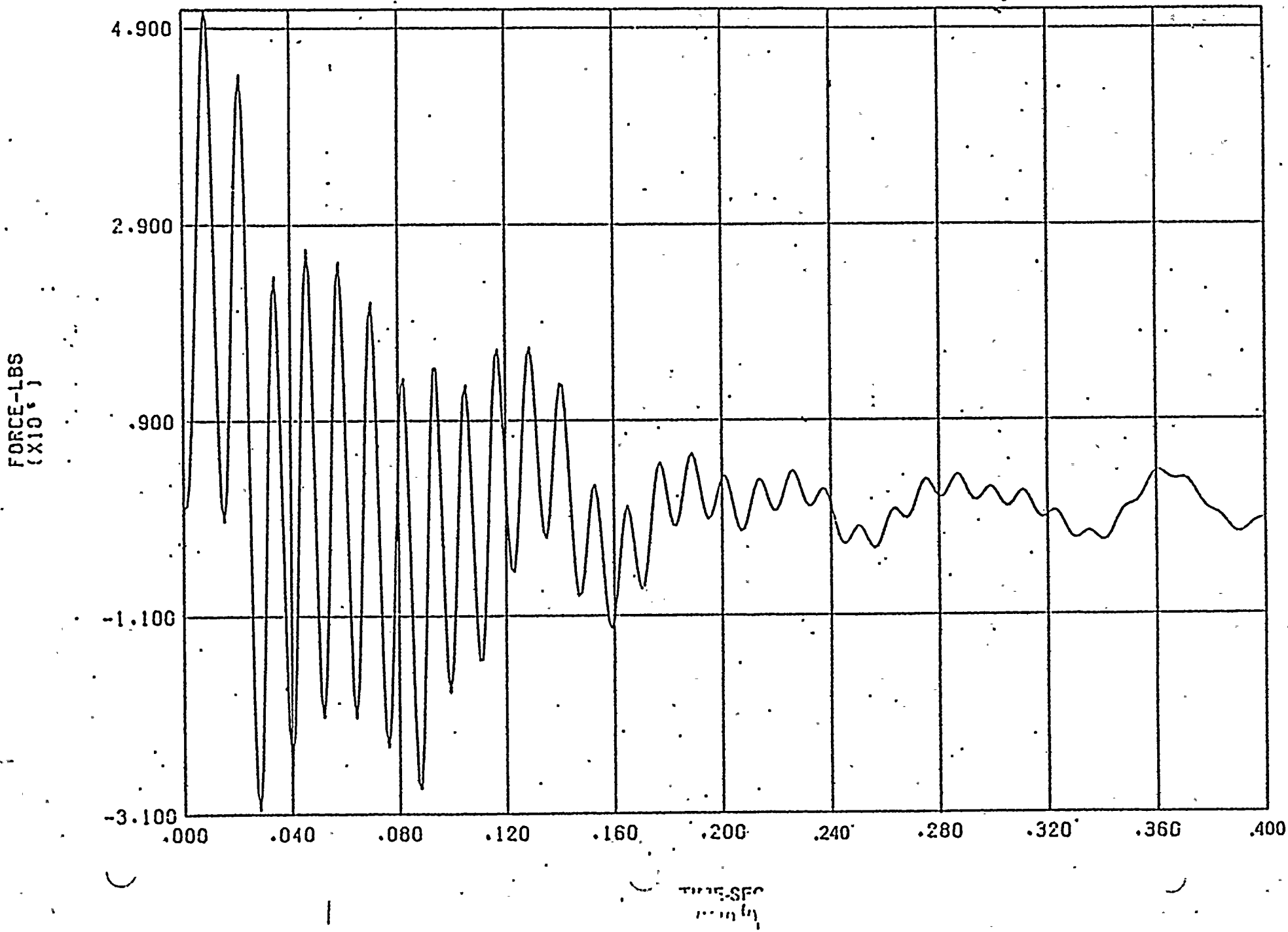

FIGURE 11

GENERIC PLANT COLD LEG BREAK CORE SUPPORT

BARREL TOTAL LOADS PERPENDICULAR TO HOT LEGS

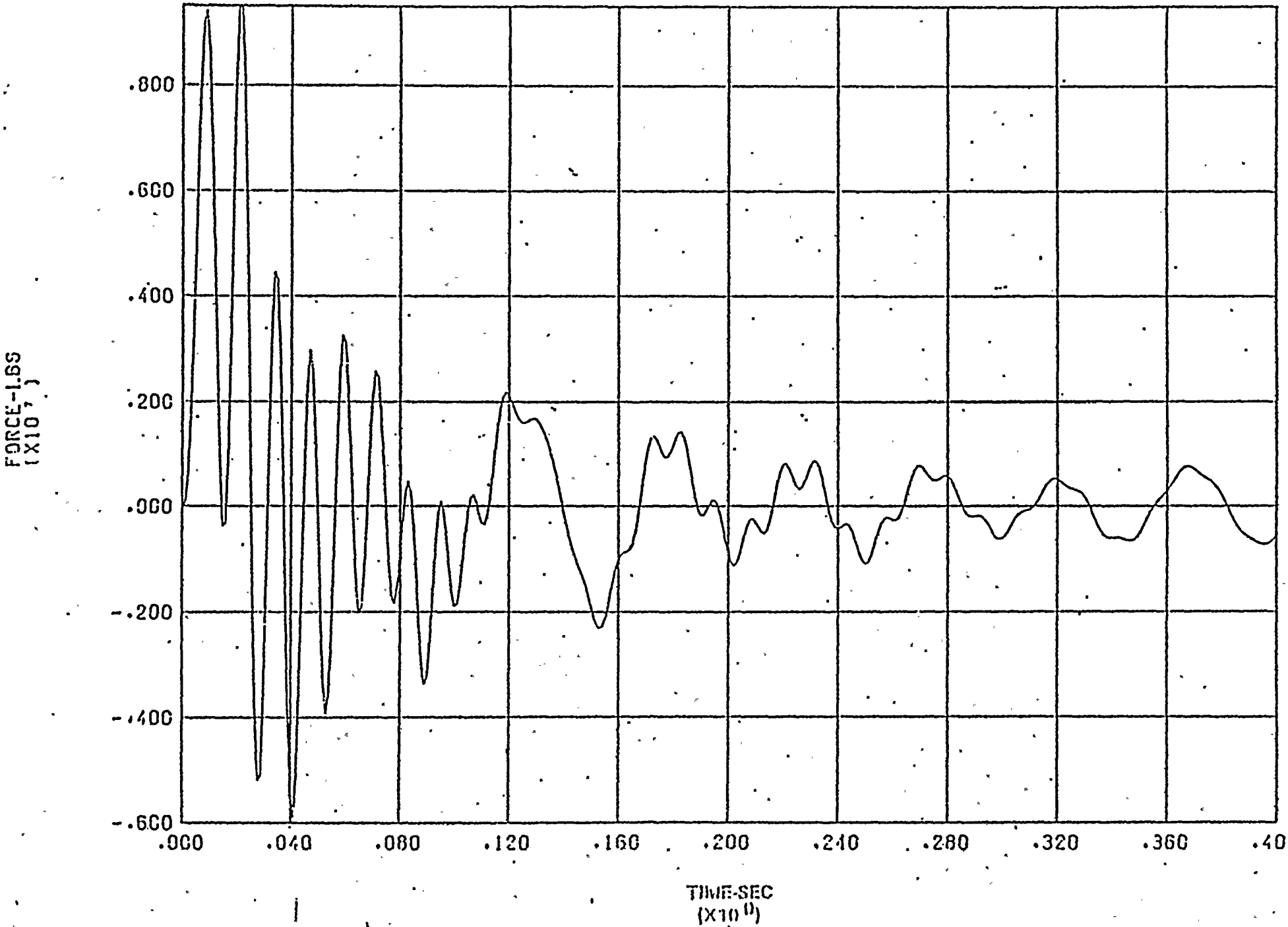

Figure 12

TOTAL INTERNAL FORCE ON THE CSB (X-COMPONENT)

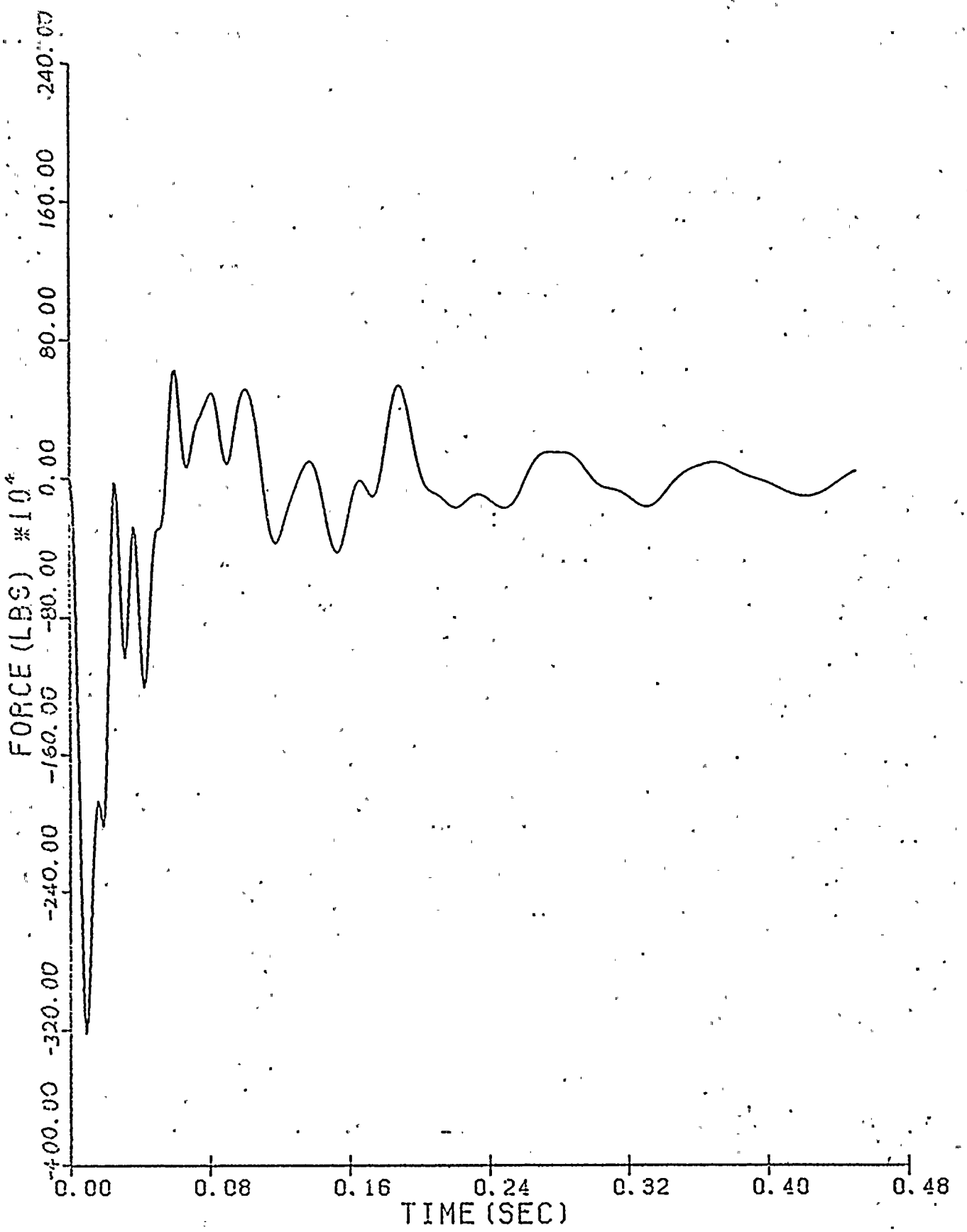

Figure 13

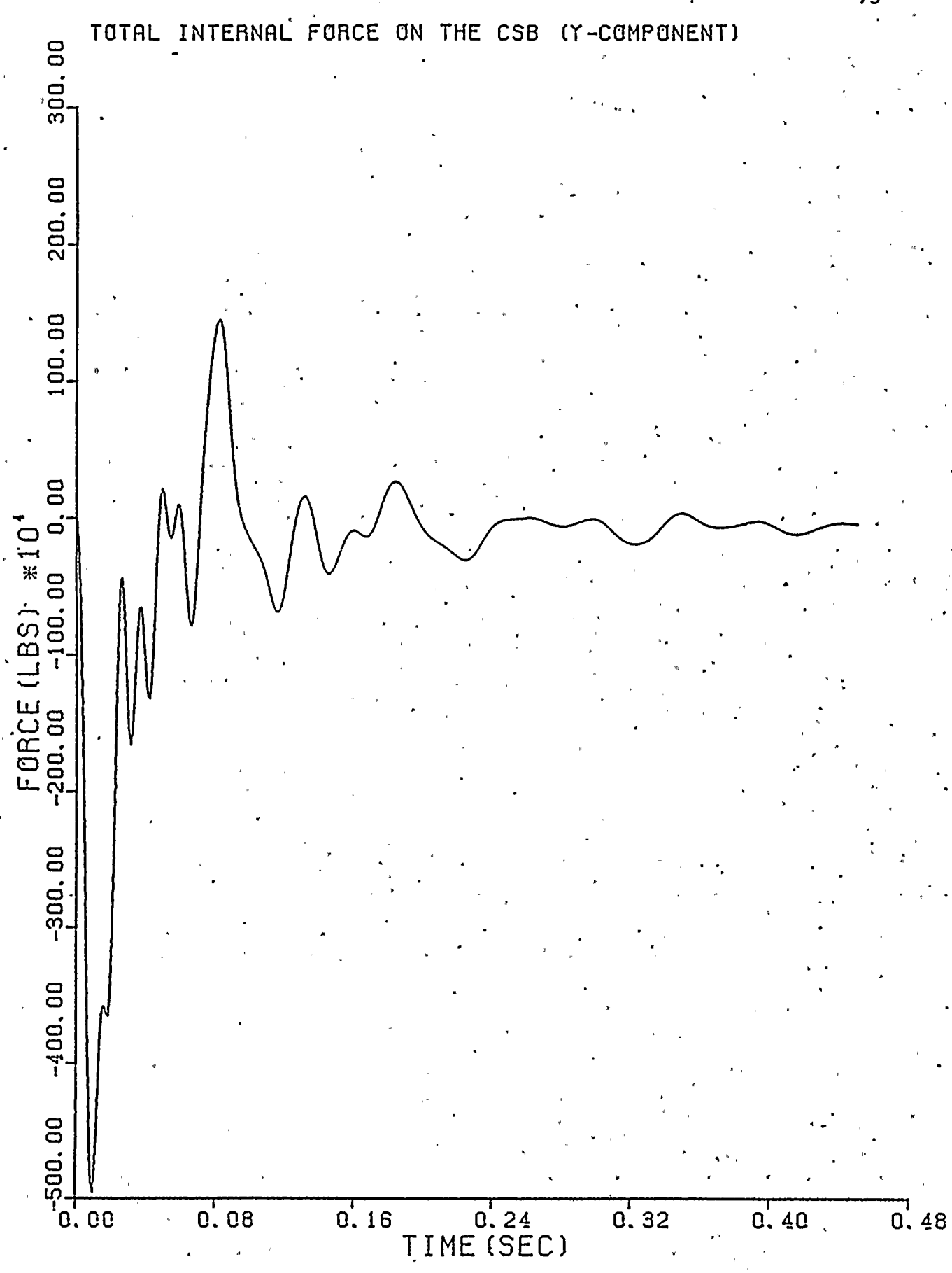
TOTAL INTERNAL FORCE ON THE CSB (Y-COMPONENT)
FORCE (LBS) *10⁴
300.00
200.00
100.00
0.00
-100.00
-200.00
-300.00
-400.00
-500.00
0.00
0.08
0.16
0.24
0.32
0.40
0.48
TIME (SEC)

FIGURE 14

GENERIC PLANT HOT LEG BREAK LATERAL CROSSFLOW LOADS ON CEA SHROUDS

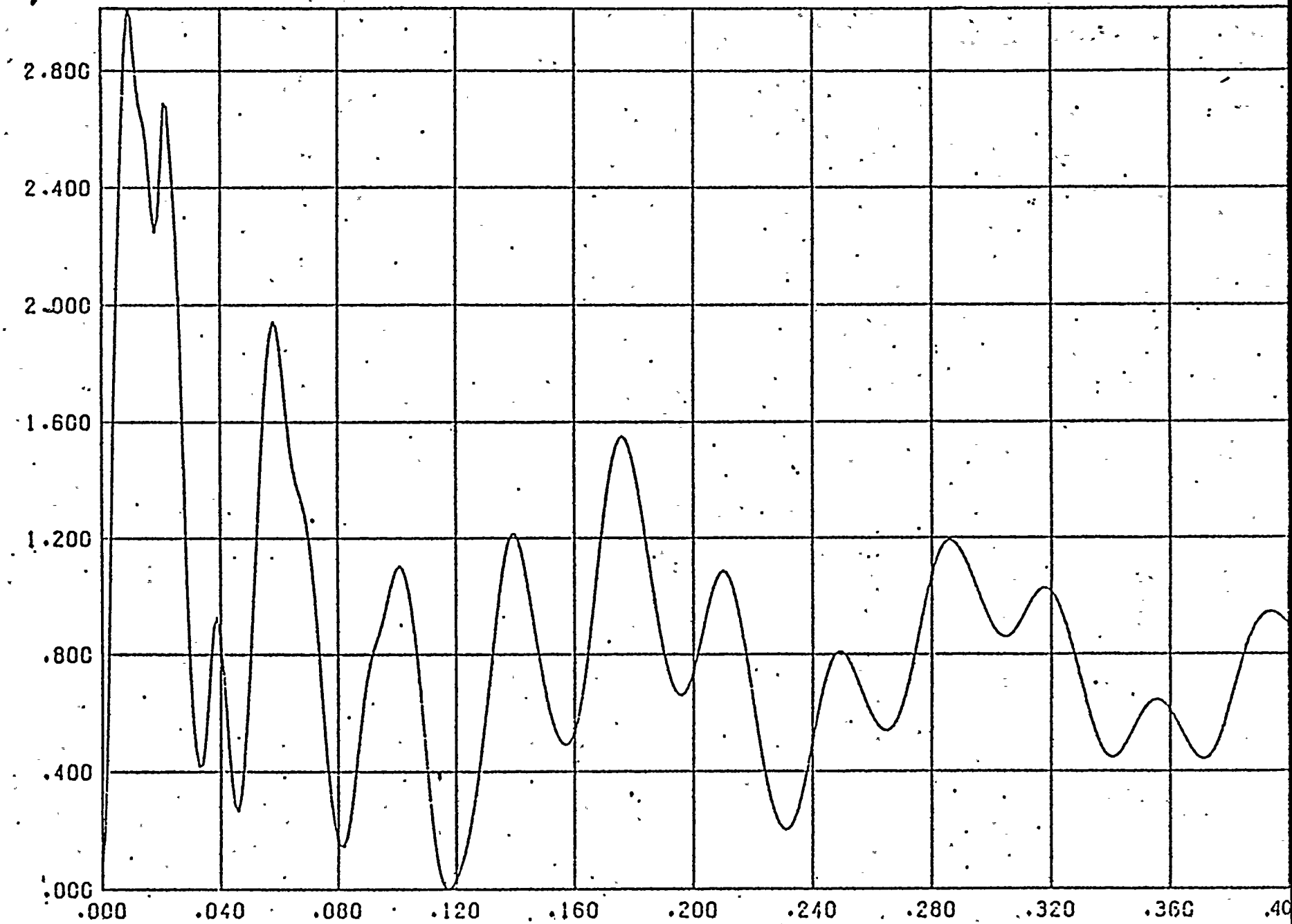

FIGURE 15

GENERIC PLANT REDUCED INTERNALS MODEL

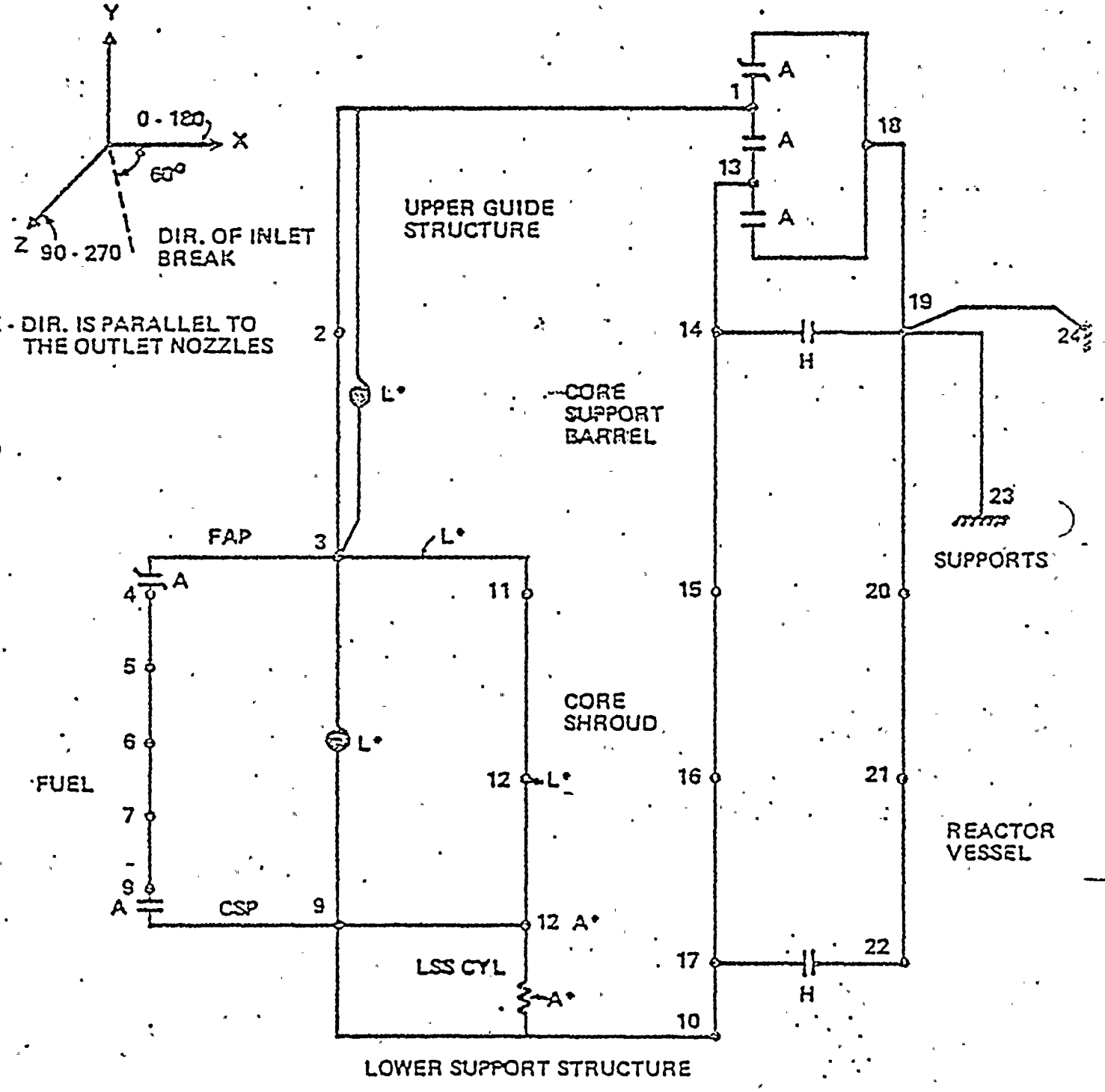

LEGEND:

A = AXIAL GAP

H = HORIZONTAL GAP

INDICATES AN AXIALLY PRELOADED COUPLING

L* = LATERAL MODEL ONLY

A* = AXIAL MODEL ONLY

FIGURE 16

GENERIC PLANT CSB
FINITE ELEMENT MODEL FOR
COLD LEG BREAK RESPONSE ANALYSIS

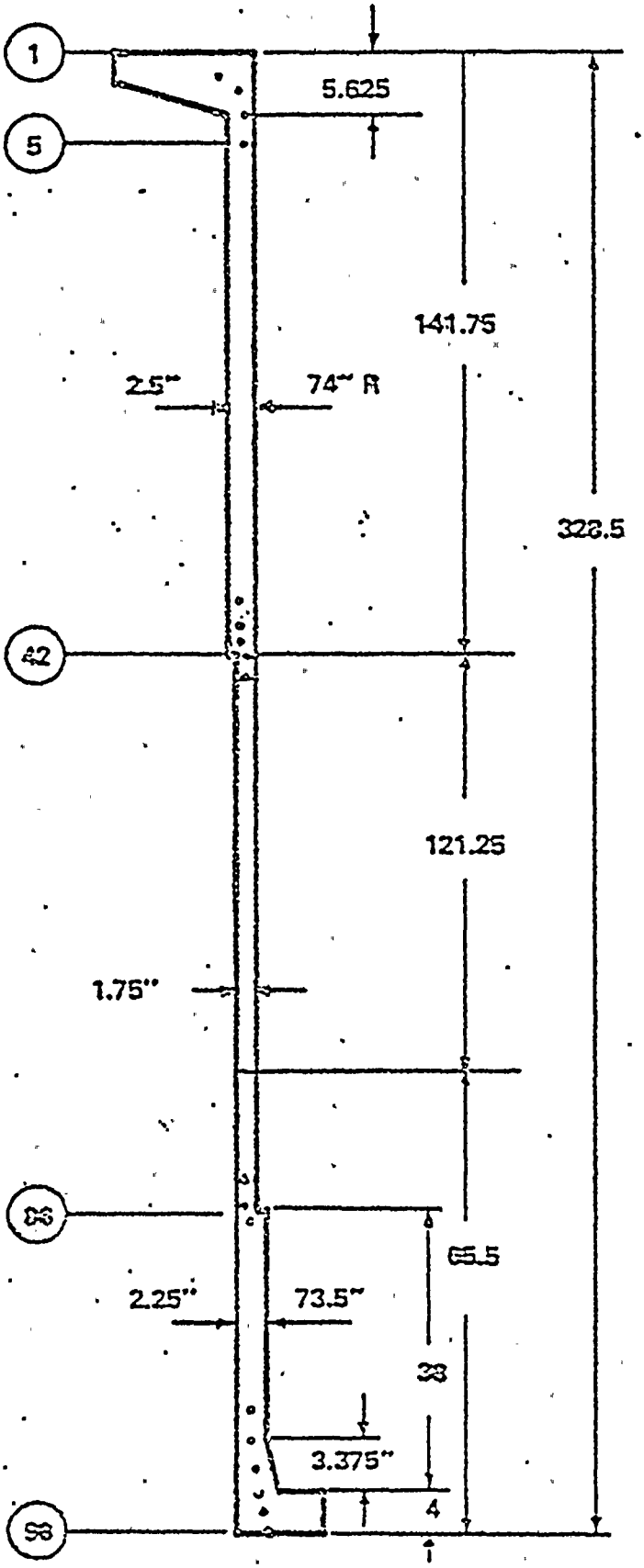

FIGURE 17

GENERIC PLANT CSB
FINITE - ELEMENT MODEL
FOR STABILITY ANALYSIS

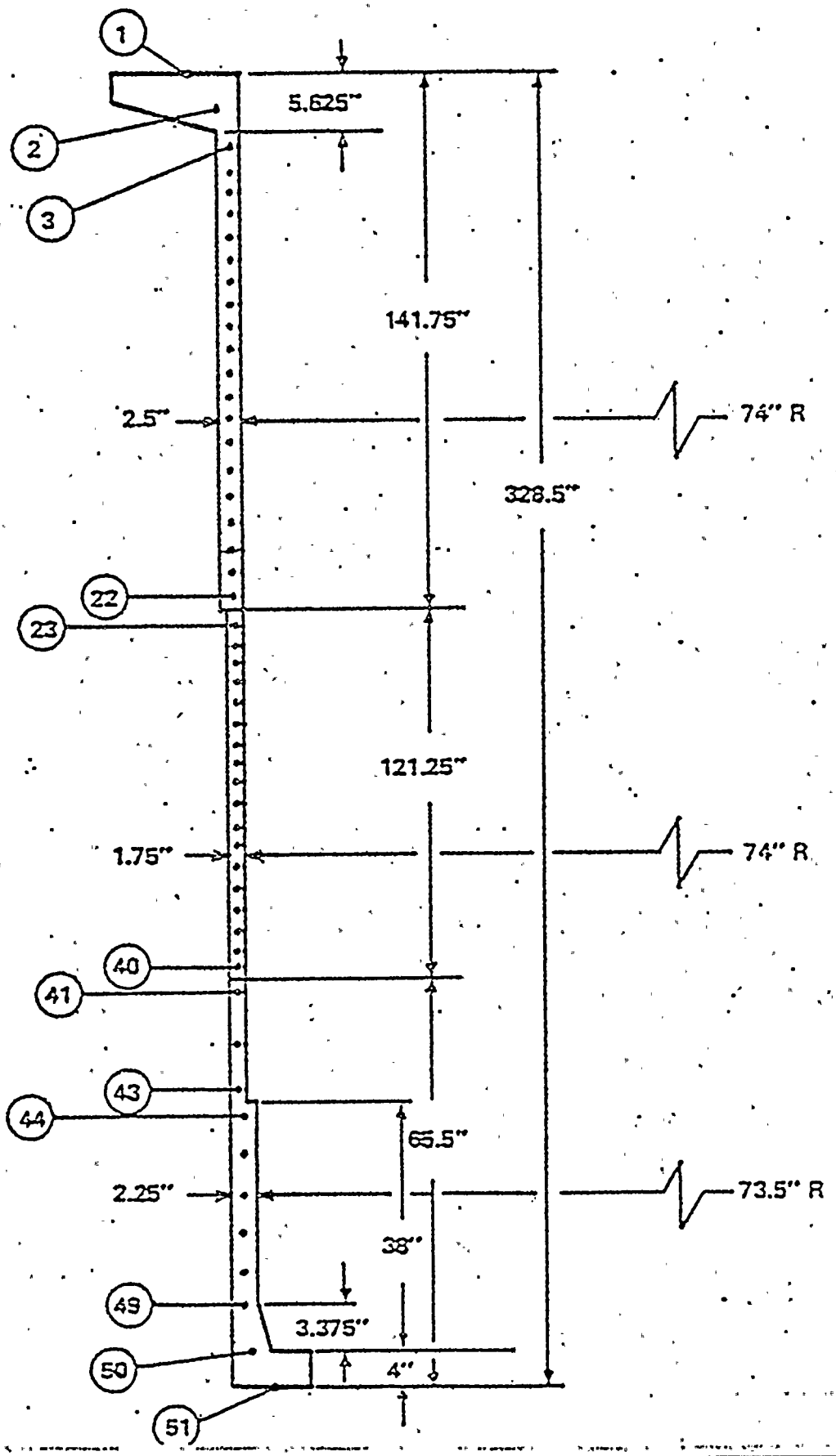

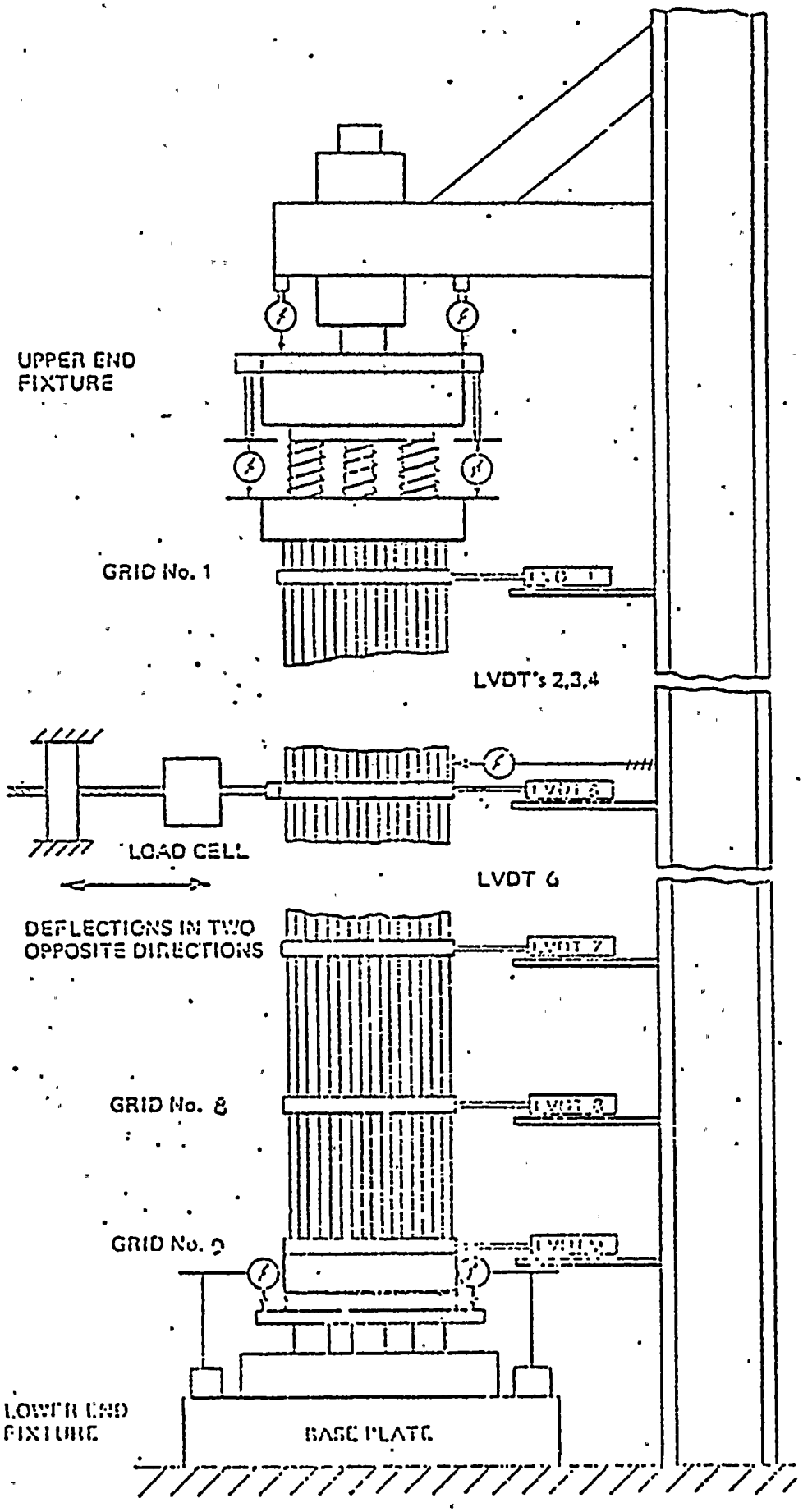

FIGURE 18

TEST SET-UP FOR LATERAL LOAD DEFLECTION TEST

RV OUTLET NOZZLE GUILLOTINE BREAK

AREA ANALYSIS

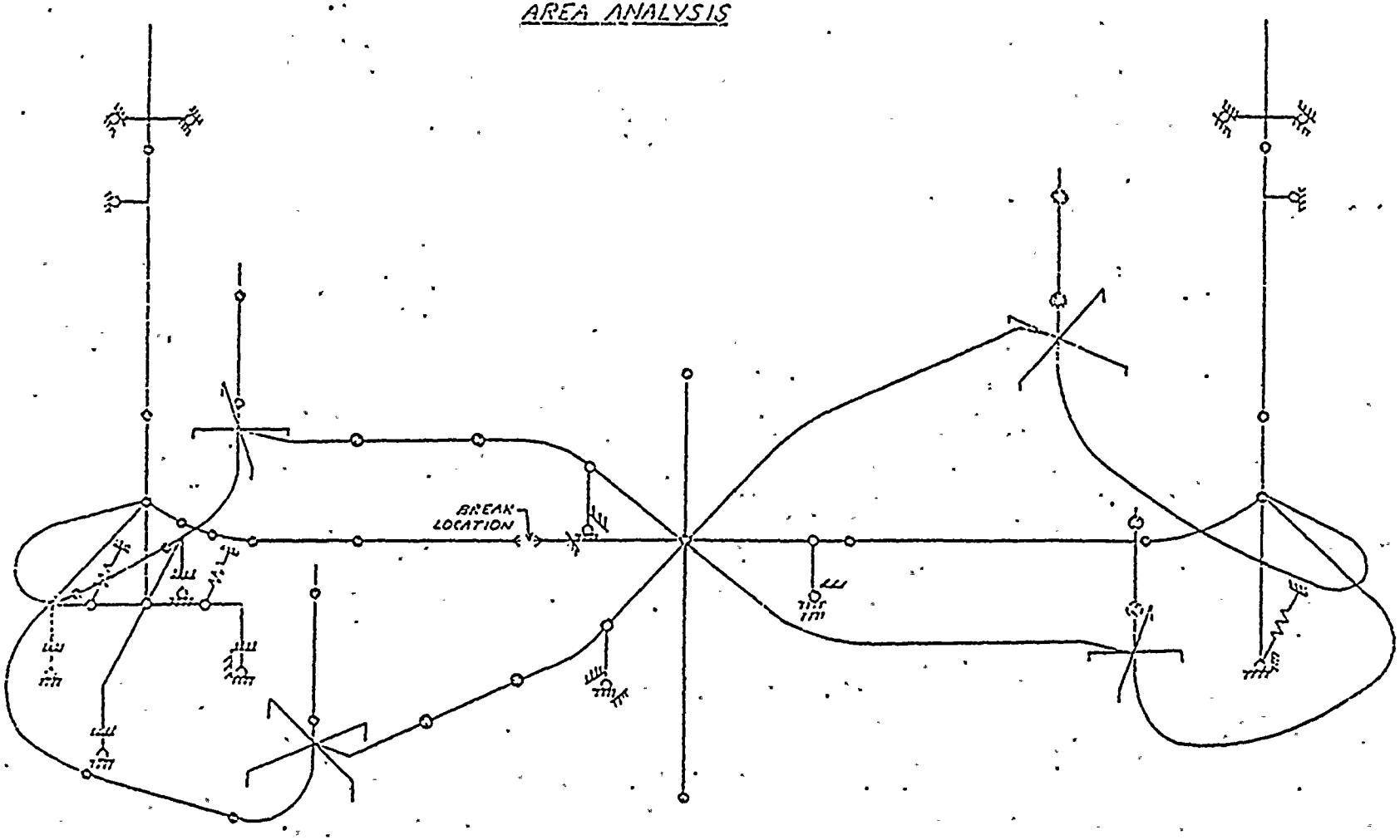

Figure 19a

RV INLET NOZZLE GUILLOTINE BREAK

AREA ANALYSIS

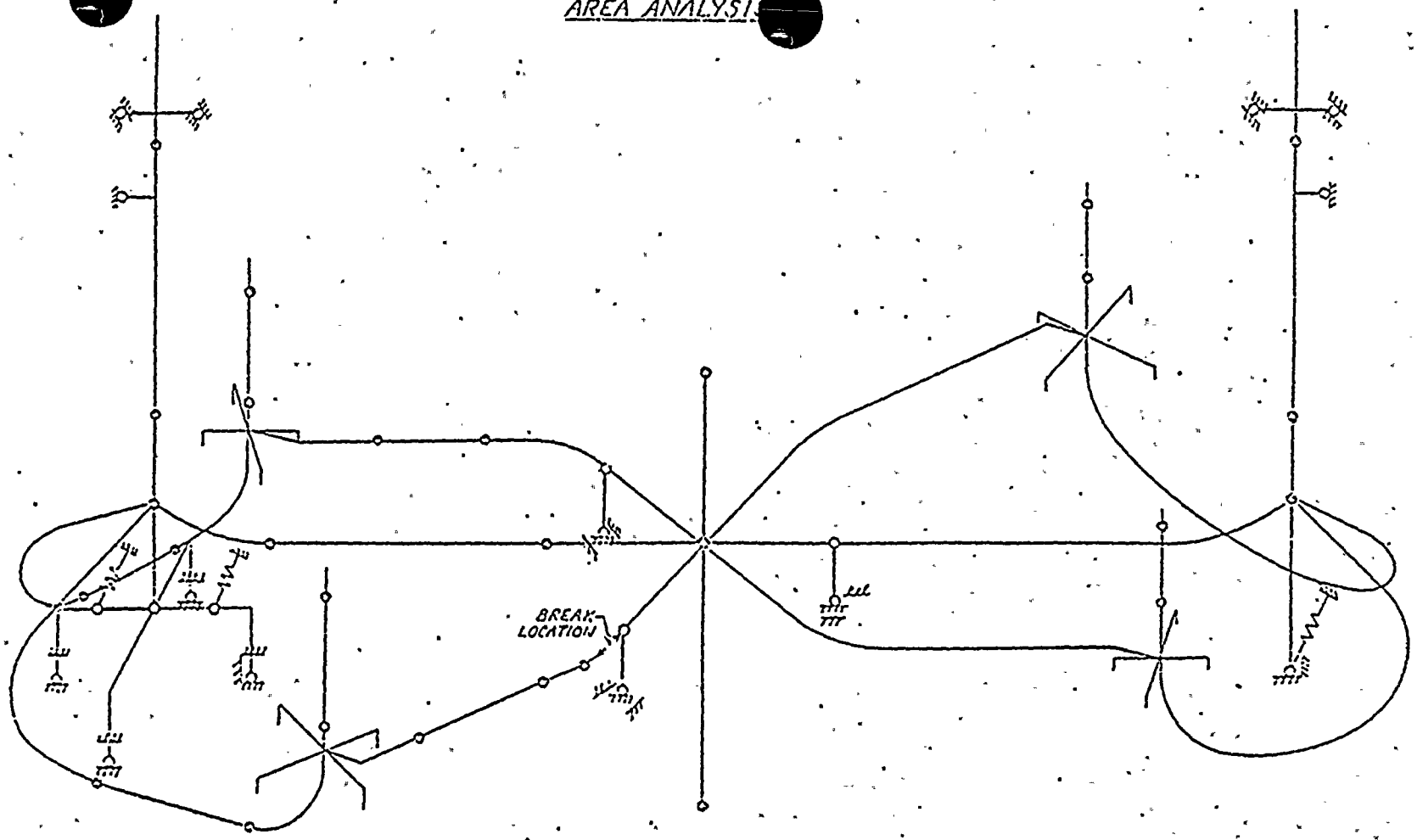

Figure 19b

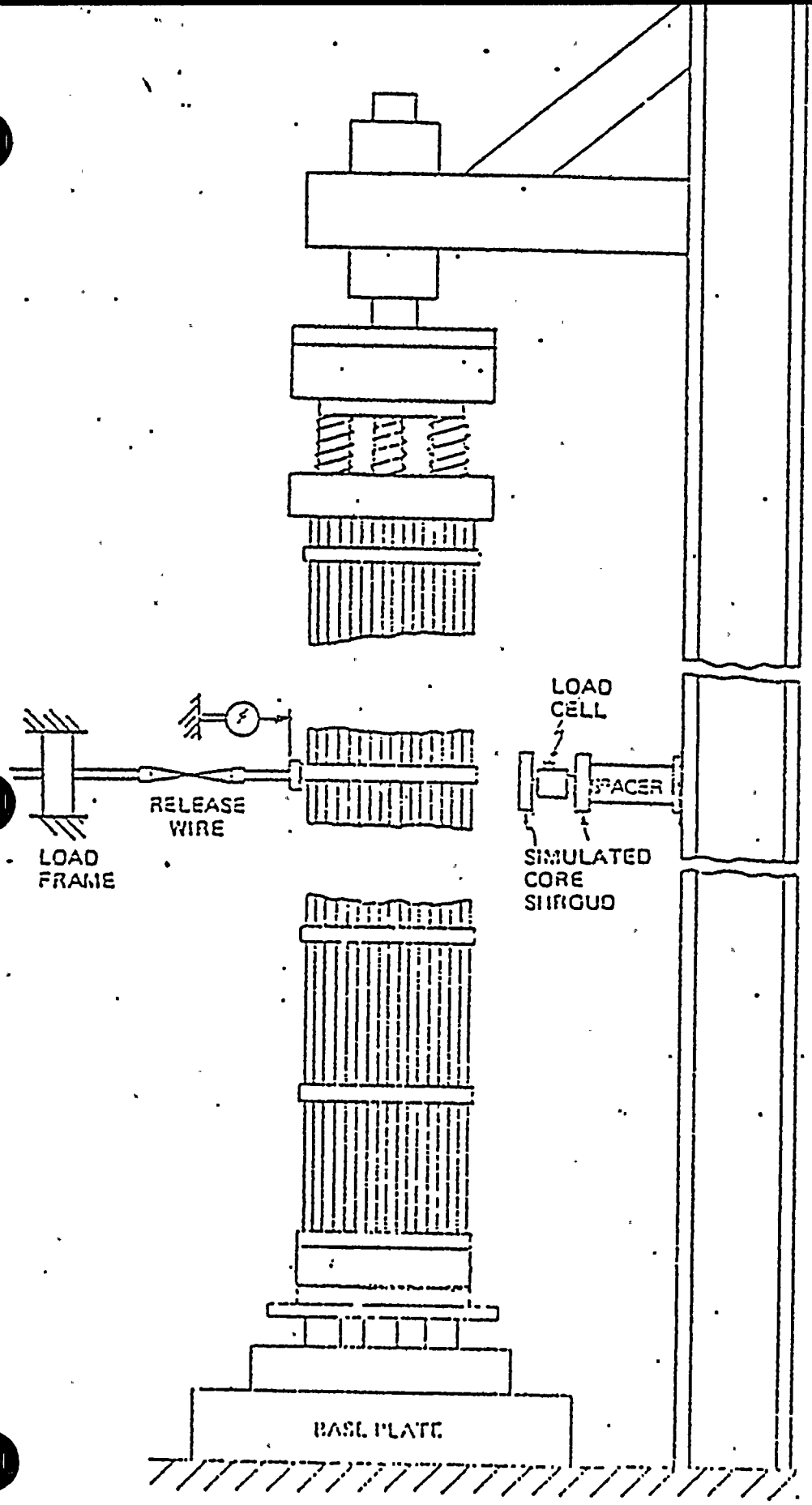

TANK FOR TESTING IN WATER ENVIRONMENT NOT SHOWN

FIGURE 20

TEST SET-UP FOR PLUCK VIBRATION AND PLUCK IMPACT TESTS